Journal of Waterway, Port, Coastal, and Ocean Engineering. Submitted April 22, 2013; accepted September 13, 2013; posted ahead of print September 16, 2013. doi:10.1061/(ASCE)WW.1943-5460.0000237

ENGINEERING MODELING OF WAVE TRANSMISSION OF REEF BALLS™

Mariano Buccino[1], Ilaria Del Vita[2], Mario Calabrese[3]

Abstract

Reef Balls™ are hemispherical concrete units, which feature pH-neutralized concrete as well as specialized surface textures to promote the growth of marine life. *Reef Balls*™ can be arranged in different layouts to form submerged breakwaters, even of significant width. Although structures formed with *Reef Balls* have been employed for the protection of several top quality sites, no well-established design tool exists for the prediction of wave transmission behind them. In this study a set of equations were proposed, based on the *conceptual approach* developed by *Buccino and Calabrese* (2007). The expressions were validated by more than 300 experimental data, from physical model tests conducted at two different laboratories. The new predictive model showed a number of encouraging properties, such as a high determination index, R^2, the normality of the residuals and a constant standard error with respect to the structure layout.

Keywords: Submerged Breakwaters, Reef Balls, Wave Transmission, Environmentally friendly units, Physical model tests.

[1] Department of Civil, Architectural and Environmental Engineering, University of Naples "Federico II". via Claudio 21, 80125 Naples (Italy). E-mail: buccino@unina.it.

[2] Department of Civil, Architectural and Environmental Engineering, University of Naples "Federico II". via Claudio 21, 80125 Naples (Italy). E-mail: ilaria.delvita@gmail.com.

[3] Department of Civil, Architectural and Environmental Engineering, University of Naples "Federico II". via Claudio 21, 80125 Naples (Italy). E-mail: calabres@unina.it

Journal of Waterway, Port, Coastal, and Ocean Engineering. Submitted April 22, 2013; accepted September 13, 2013; posted ahead of print September 16, 2013. doi:10.1061/(ASCE)WW.1943-5460.0000237

Nomenclature

The following symbols are used in this paper (Figure 1):

Figure 1. Definition sketch of the main variables.

A_0	[-]	Scale parameter of Armono's formula.
B_m	[m]	Crest width of the rubble mound foundation.
B_t	[m]	Nominal crown width.
B_t^*	[m]	Effective crown width.
D_{n50}	[m]	Nominal median diameter of the rubble mound foundation (armor or core).
D_R	[m]	Base diameter of the *Reef Ball* modules.
d	[m]	Water depth.
F	[m]	Submerged depth of the rubble mound foundation.
G	[-]	Dissipation index.
g	[m/s^2]	Gravity acceleration.
h_m	[m]	Height of the rubble mound foundation.
h_R	[m]	Height of the *Reef Ball* modules.
h_s	[m]	Height of the entire structure.
h_{se}	[m]	Equivalent structure height.
H_{si}	[m]	Incident significant wave height.

H_{st}	[m]	Transmitted significant wave height.
L_{0p}	[m]	Peak deep water wavelength.
n	[-]	Number of *Reef Ball* rows at the top of the structure.
R_c	[m]	Crest freeboard (to be taken positive).
R_{ce}	[m]	Equivalent crest freeboard.
$tg\alpha_{off}$	[-]	Front slope of the rubble mound foundation.
T_p	[sec]	Peak period.
v	[-]	Configuration factor.

Introduction

Submerged breakwaters are rubble mound barriers with crests below the mean water level, generally armored with rock. They may stretch along the shore for several kilometers, and in most cases have gaps that allow boats to reach the shore. The purpose of these structures is to dissipate some of the wave energy. The degree of protection afforded to the coast is usually measured by the *transmission coefficient,* K_t, which is the ratio between the wave height immediately shoreward of the barrier (transmitted wave height) and that immediately seaward of it (incident wave height). In many countries of the world, Italy, Spain and Japan among them, submerged breakwaters are considered the sole structural measure for shore erosion control that is consistent with a policy of protection of the natural and historical beauty of coastal areas. For this reason, their structural, hydraulic and environmental responses have been intensively investigated in the recent decades. The EU-funded project *DELOS* (*Lamberti, 2005, Burcharth et al., 2007*) is among the most fruitful research efforts.

Journal of Waterway, Port, Coastal, and Ocean Engineering. Submitted April 22, 2013; accepted September 13, 2013; posted ahead of print September 16, 2013. doi:10.1061/(ASCE)WW.1943-5460.0000237

In spite of their undoubted advantages, conventional submerged breakwaters generally require the quarrying of a large amount of rocky material; in addition to the expense, especially when the structures are long and wide, quarrying inflicts noticeable harm to the environment, and for this reason, it is often forbidden or extremely difficult to achieve.

One solution is the use of *environmentally friendly* concrete units. In addition to reducing the volume of rock to be employed, *environmentally friendly* concrete units are able to interact with marine life, favoring a number of recreational activities, such as surfing, snorkeling and fishing. This may ultimately increase the appeal of the beach, generating economic benefits. In this study, we analyze one of the most popular *environmentally friendly units* for submerged breakwaters, the *Reef Ball*™ (*www. Reefball.org*) (*RB*), with respect to its wave energy transmittance.

Reef Balls (*Barber, 2001; Harris, 2007*) are hemispherically shaped artificial reef modules (Figure 2a), originally designed for biological enhancements; their use was later expanded to shoreline stabilization. They are available in various sizes and shapes (Table 1) and can be arranged in rows (Figure 2b), to form submerged barriers of significant width. *RBs* feature a pH neutralized concrete, specialized surface textures and numerous holes to promote equilibrated growth of flora and fauna. The modules are easy to install and can be constructed locally, or on site. From a structural point of view *RBs* are hardly flipped over, because of their low center of mass, whereas horizontal sliding is prevented through anchoring systems of different types, such as cones, spikes, piles and concrete mats. The latter can also prevent settlement into soft bottoms.

Even though submerged barriers composed of *RBs* have been employed to defend a number of high quality sites, such as Marriott Beach Resort (Cayman Islands) and Gran Dominicus Resort (Dominican Republic), no reliable design equation exists to calculate the transmission coefficient in their lee.

Journal of Waterway, Port, Coastal, and Ocean Engineering. Submitted April 22, 2013; accepted September 13, 2013; posted ahead of print September 16, 2013. doi:10.1061/(ASCE)WW.1943-5460.0000237

Figure 2. (a*) Reef Balls*; (b) *Reef Balls* arranged in rows at the Gran Dominicus Resort (Dominican Republic). Source: www. Reefball.org.

Table 1. *Reef Ball* characteristics. Source: www. Reefball.org.

Although wave attenuation is only one of the complex mechanisms that control the wave-barrier interaction, it is one of the primary effects from an engineering point of view. The lack of an effective predictive tool may inhibit the use of the modules for shore protection purposes.

The only model proposed to date to estimate K_t is that suggested by *Armono* (2002); however, *Armono*'s model is developed from the analysis of a single data set and refers to structures where the *RB*s are assembled in unusual ways. In this study, *Armono*'s data have been added with a new set of random wave experiments conducted for a shore protection project planned to protect 63rd Street, Miami Beach, FL (*Ward, 2012*, in press). Because *Armono's* model is not adequate to fit the entire data base, the *conceptual approach* (*CA*), proposed by *Buccino and Calabrese* (2007) for conventional breakwaters, was applied to the data. Among the many available formulae for common structures (*d'Angremond et al., 1996; Seabrook and Hall, 1998, Briganti et al., 2004; van der Meer et al., 2005; Goda and Ahrens, 2008; Tomasicchio et al., 2013*), *CA* was chosen because the predictive equations have been theoretically deduced, although on the basis of a very simplified calculation scheme; consequently, the parameters each have a physical meaning, which may aid the analysis and the discussion.

Description of the data base

The data base employed in this study is created by two ensembles of 2D random wave experiments, conducted at the *Queen's University Coastal Engineering Research Laboratory* (*QUCERL*, Canada) and at the USACE *Engineering Research and Development Center Coastal and Hydraulics Laboratory* (*ERDC/CHL*, USA). To the authors, knowledge these tests represent, to date, the sole systematic investigations carried out to study wave transmission through *RBs*. The

Journal of Waterway, Port, Coastal, and Ocean Engineering. Submitted April 22, 2013; accepted September 13, 2013; posted ahead of print September 16, 2013. doi:10.1061/(ASCE)WW.1943-5460.0000237

QUCERL experiments are described in *Armono* (2002) and in *Armono and Hall* (2003); the ERDC/CHL experiments are presented herein for the first time, with the cooperation of *Donald L. Ward* (Coastal Engineering Research Center).

The QUCERL tests

The *QUCERL* test data form the calibration set of Armono's prediction model, which is, to date, the unique design tool proposed specifically for *RBs*. The experiments were performed in a flume 47 m long, 0.9 m wide and 1.2 m deep, using a flap-type wave-maker. The *Reef Balls* were located on a horizontal bottom 17 m from the paddle. The modules height, h_R, was 0.13 m with a base diameter, D_R, of 0.20 m; the weight of the units ranged from 2.189 to 2.944 kg, and the number of holes over the lateral surface was approximately 20 per unit. Table 1 suggests that these characteristics roughly correspond to *Pallet Balls* scaled down at a 1:7 ratio.

RBs were arranged in different layouts. In some cases the modules were seated directly on the bottom (layout *BS*). In other cases, the units were placed onto the crown of a conventional rubble mound (layout *B*). As shown in Figure 3a, the layout *BS-3* utilizes 3 levels of *Reef Balls*; the second one is arranged upside-down to give a good interlocking with the first layer and to provide a base for the top level (*Armono and Hall*, 2003). The configuration *BS-2* (Figure 3b) is obtained from *BS-3* by simply removing the third layer.

Figure 3. (a) Layout *BS-3*; (b) Layout *BS-2*. Source: *Armono* (2002).

As far as the configurations of type "*B*" are concerned, the *Reef Balls* have been assembled in 1 or 2 levels. In the first case, the modules may cover the entire crown (layout *BF-1* Figure 4a) or only part of it (layout *BP-1* Figure 4b). *BF-2* is the case where two layer of *RBs* have been used (Figure 4c). The rubble mound was placed on a core with $D_{n50} = 0.01$ m and two layers of armor with

Journal of Waterway, Port, Coastal, and Ocean Engineering. Submitted April 22, 2013; accepted September 13, 2013; posted ahead of print September 16, 2013. doi:10.1061/(ASCE)WW.1943-5460.0000237

D_{n50} = 0.037 m; the height of the structure (h_m), the crown width (B_m) and the slope angles ($\alpha_{off.}$ and $\alpha_{in.}$) were constant throughout the tests.

For each configuration tested, Table 2 reports the number of available data, the number of rows of *RBs* at the top of the structure (*n*) and the ranges of water depth (*d*), significant incident wave height (H_{si}), peak period (T_p) and K_t.

Figure 4. (a) Configuration *B-F1*; (b) configuration *B-P1*; (c) configuration *B-F2*.

Source: *Armono* (2002).

Table 2. Synthesis of the *QUCERL* tests.

The main limitation of the *QUCERL* data set is that the most commonly employed *BS* configuration, a single layer of *RBs* placed directly on the bottom (Figure 1b and Figure 2b), was not tested. Additionally, for each layout investigated, the width of the structure was not changed; thus, the effect of this primary variable could not be analyzed properly.

The *ERDC/CHL* data set partially fills those gaps.

The ERDC/CHL tests

The *ERDC/CHL* experiments *(Ward*, unpublished report*)* were carried out to optimize the design of an offshore submerged breakwater of *RBs* with the purpose of defending 63rd Street, Miami Beach (FL, USA). This project was part of the *National Shoreline Erosion Control Development and Demonstration Program*, which aims at advancing the state of the art of shoreline protection, through a series of demonstrative projects of innovative solutions.

Journal of Waterway, Port, Coastal, and Ocean Engineering. Submitted April 22, 2013; accepted September 13, 2013;
posted ahead of print September 16, 2013. doi:10.1061/(ASCE)WW.1943-5460.0000237

The experiments were conducted in a wave basin 51.82 m long, 30.48 m wide and 1.21 m deep, a 27 m wide multi-directional wave generator. At nearly 15 m from the paddle, the tank was partitioned to form a 20.73 m by 2.44 m flume, normal to the generator. The flume's profile, which reproduced the topography of the site at a 1:10 length-scale, included a 1:20 slope, for 4.87 m, followed by a 1:250 slope, for 9.75 m, and then a 1:7.5 slope for 4.87 m.

1:10 models of *Goliath Balls* (Table 1) were installed directly on the bottom, arranged on a single level (*BS-1*), according to the typical configuration of the *RBs*. The modules were placed in rows on the 1:250 slope, with the offshore row beginning where the slope transitioned from 1:20 to 1:250. Different configurations were obtained by varying the spacing between the units, both in the direction of the wave propagation (*cross-shore*) and normal to it (*along-shore*). Moreover, the number of rows (*n*) has been changed to investigate the role of the structure width.

The characteristics of the layouts are displayed in Table 3. The layout *BS-1a* has 10 modules in each row, with an alongshore spacing of 0.055 m. Up to 7 rows have been used, with the cross-shore spacing also set at 0.055 m. Each row of *RBs* was added in such a way that the center of each unit was aligned with the gap between two units in the preceding row. The layout *BS-1b* is obtained from *BS-1a* by removing the even rows. Consequently, the modules are now perfectly aligned cross-shore. The structure *BS-1c* is formed from *BS-1a* with *n = 7*, after eliminating row number 2. The configuration *BS-1d*, is identical to *BS-1b*, but the modules are not aligned. The structure *BS-1e* includes 3 rows with no spacing between the units. Finally, the layout *BS-1f* is obtained from *BS-1b*, by halving the number of modules in each row.

Table 3. Summary of *ERDC/CHL* tests.

Wave transmission for the BS configurations

Armono's equation

The most natural starting point for this research is Armono's equation (*Armono, 2002*), which, to date, is the only formula valid for submerged breakwaters with *RBs*. Analyzing the *QUCERL* data, and comparing different functional forms, the author derived the following model:

$$Y = 1 + A_0 X \tag{1}$$

where:

$$\begin{cases} Y = \dfrac{1}{K_t} \\ X = \left(\dfrac{H_{si}}{gT_p{}^2}\right)^{0,901} \left(\dfrac{B_{bR}}{gT_p{}^2}\right)^{-0,413} \left(\dfrac{h_s}{B_{bR}}\right)^{-1,013} \left(\dfrac{h_s}{d}\right)^{4,392} \end{cases} \tag{2}$$

In Eq. (2), h_s represents the structure height (Figure 1) and B_{bR} equals the sum of D_R at the structure basement. Eq. (1) depends on 4 predictors that have been selected by means of dimensional analysis. The predictors are powered at constant exponents, whereas the *scale factor* A_0, of the order of 10, varies as a function of the layout (Table 4).

Table 4. Values of Armono's scale factor.

<u>*Comparison with ERDC/CHL dataset*</u>

Unlike the *QUCERL* experiments (Figure 5a), *ERDC/CHL* data do not corroborate Armono's approach (Figure 5b); when plotted on the *X-Y* plane, the points are split into two sub-arrays, irrespective of the layout. Moreover, in some cases (layouts *BS-1c, BS-1e* and *BS-1f*) there is no correlation at all between *X* and *Y* (Figure 6).

Figure 5. (a) Armono's equation vs. *BS-2* data. (b) Armono's equation vs. *ERDC/CHL* data.

Figure 6. Armono's equation vs. layouts *BS-1c*, *BS-1e* and *BS-1*f.

Journal of Waterway, Port, Coastal, and Ocean Engineering. Submitted April 22, 2013; accepted September 13, 2013;
posted ahead of print September 16, 2013. doi:10.1061/(ASCE)WW.1943-5460.0000237

In Figure 5a, the *QUCERL* data (layout *BS-2*) exhibit a certain curvature around the mean trendline, especially when *X* is small. This suggests that Armono's equation might suffer from some inherent lack of fit, at least with respect to the *BS* arrangements. This feature deserves to be properly analyzed prior to looking for possible corrections.

Possible reasons for the lack of fit

The technique employed in the following is the *added variable plot* (*AVP*), which is frequently used in the field of regression analysis (*Draper and Smith, 1981*). In *AVP*, the effects of the predictors in a model are evaluated by performing partial regressions with respect to some of the variables and then plotting the residuals against the other variables. To begin, Armono's equation is generalized to a first order linear model as follows:

$$Y_t = a_0 + a_1 X_1 + a_2 X_2 + a_3 X_3 + a_4 X_4 \tag{3}$$

where:

$$Y_t = \ln\left(\frac{1}{K_t} - 1\right);\ X_1 = \ln\left(\frac{h_s}{d}\right);\ X_2 = \ln\left(\frac{h_s}{B_{bR}}\right);\ X_3 = \ln\left(\frac{H_{si}}{g{T_p}^2}\right);\ X_4 = \ln\left(\frac{B_{bR}}{g{T_p}^2}\right) \tag{4}$$

According to the *AVP*, a regression of Y_t on X_1 is performed first. As shown in Figure 7a, the scatter plot is nearly linear, and the slope of the fitted straight line, 4.83, is close to that proposed by Armono (4.32, see Eq. (2)). Although the value of the R^2 statistics is low (0.30), the regression is absolutely significant, with a p-value of the *F* statistics equal to 6.6 x 10^{-10}.

To test the role of the second predictor, X_2 is regressed on X_1 to remove any supplementary effect of the latter; then the residuals of this regression, e_{x2}, are calculated. Because no relationship was found between the variables, the residuals equal the difference between the values of X_2 and their arithmetic mean.

Journal of Waterway, Port, Coastal, and Ocean Engineering. Submitted April 22, 2013; accepted September 13, 2013;
posted ahead of print September 16, 2013. doi:10.1061/(ASCE)WW.1943-5460.0000237

Figure 7. *AVP* analysis of *QUCERL* data (*BS* layouts).

In Fig. 7b, e_{x2} are shown on the abscissa and the residuals of the regression of Figure 7a, e_{Y1}, are on the ordinate. In this case, the linear trend is a Hobson's choice, as there are only two values of e_{x2}. This is because B_{bR} is the same (1 m) for *BS-2* and *BS-3* thus, the variance of X_2 depends only on h_s. The single value for B_{bR} is a major defect of the *QUCERL* data. Nonetheless, the new straight line in Figure 7b, which passes through the origin by construction, can be added to that of Figure 7a; resulting in new estimates for Y_t and new residuals (e_{Y2}).

The same procedure is repeated to assess the value of adding the variable X_3. In Figure 7c, the residuals e_{X3} (X_3 is independent of X_1 and X_2) are plotted vs. e_{Y2}. Despite the assumption made by Armono, the relationship appears to be generally nonlinear (dashed curve), explaining the aforementioned convex shape of the experimental points in Figure 5a. However, following Armono's approach, e_{Y2} is initially fit with a straight line. After adding the new component to the previous results, the new residuals, e_{Y3}, can be obtained.

The variable X_4 is significantly correlated to X_3 ($R^2 = 0.60$); yet, even elimineting this dependence, regressing X_4 on X_3, the residuals e_{X4} still show a small ($R^2 = 0.15$) but significant linear relationship with e_{Y3} (Figure 7d). According to Armono's equation, the slope of the fitted straight line is negative, meaning that the transmission coefficient increases with the reef width to wavelength ratio. This feature is questionable from a physical point of view.

The apparent inconsistency can be explained by noting that since B_{bR} is constant, X_4 depends only on the wave period; thus the result of Fig. 7d indicates that X_3 is not enough to completely account for the effect of T on the transmission process, so that another predictor, dependent on wave period, should be added to the regression model. Clearly, the choice of using X_4 for that purpose appears to the authors not to be sharable and likely represents the main source of bias of Eq. (1).

Journal of Waterway, Port, Coastal, and Ocean Engineering. Submitted April 22, 2013; accepted September 13, 2013; posted ahead of print September 16, 2013. doi:10.1061/(ASCE)WW.1943-5460.0000237

<u>*A tentative correction of the model*</u>

Based on the previous discussion, Armono's model might be re-arranged as follows:

$$Y_t = b_0 + b_1 X_1 + b_2 X_2 + b_3 X_3 + b_4 X_3^2 + b_5 X'_4 \tag{5}$$

where X'_4 is a new variable, which is a function of the wave period, to be used instead of X_4. However, it has been recognized that the inclusion of such a predictor (e.g., $ln(d/gT^2)$) enhances the quality of the estimates only slightly; this was partly expected as the R^2 statistics in Fig. 7d is small. Hence, only the first 5 terms of Eq. (5) were retained. This leads to a simplification of the model and avoids introducing other variables than those suggested by Armono. After fitting <u>only the *QUCERL* data</u>, the following calibrated equation was obtained:

$$Y_t = -10.87 + 3.93 X_1 - 1.49 X_2 - 3.70 X_3 - 0.38 X_3^2 \tag{6}$$

Eq. (6) does not perform as well as Armono's formula ($R^2 = 0.88$ vs. 0.92), but the unrealistic dependence on B_{bR}/gT^2 has been removed and the nonlinear dependence on wave steepness has been accounted for, as shown by the scatter plots of the residuals shown in Figures 8a and 8b.

Figure 8. Effects of the model corrections: scatter plots of the residuals vs. X_3 for Eq. (6) (a) and the original Armono's equation (b). In the panel (c), Eq. (6) is compared to the *ERDC/CHL* data.

The nonlinear effects become more important for low values of X_3, according to the data shown in Figures 5a and 7c. However, the data splitting shown in Figure 5b seems to disappear when comparing the new model to the *ERDC/CHL* data (Figure 8c); the prediction line passes now through the bulk of the points and this might be interpreted that the model has been improved. Significant scatter still exists, which, according to Armono, could be reduced by adjusting the scale factor b_0 to each configuration separately. Thus, Eq. (5) was first re-fitted to all the data (*QUCERL+ERDC/CHL*), obtaining the following:

Journal of Waterway, Port, Coastal, and Ocean Engineering. Submitted April 22, 2013; accepted September 13, 2013;
posted ahead of print September 16, 2013. doi:10.1061/(ASCE)WW.1943-5460.0000237

$$Y_t = -9.3 + 4.07X_1 - 1.33X_2 - 3.05X_3 - 0.31X_3^2 \quad (7)$$

then the parameter b_0 was re-calculated series by series as the mean of the difference:

$$Y_{t,meas} - \left[4.07X_1 - 1.33X_2 - 3.05X_3 - 0.31X_3^2\right] \quad (8)$$

The results are summarized in Table 5 and indicate that the *ERDC/CHL* data yield a larger transmission rate on average, compared to the *QUCERL* data (remember that a logarithmic transformation has been applied to $1/K_t$); in particular, a wide spacing in the along-shore direction leads to a significant reduction of the efficiency (for *BS-1f*, b_0 = -10.26). Furthermore, the *BS-2* arrangement seems some more dissipative than *BS-3*, according to Armono's original findings (Table 4).

Table 5. Values of the parameter a_0.

This point is discussed further in the next Section.

Figure 9 reports the comparison between computed and measured K_t; the overall R^2 statistics is 0.80 and the residuals (difference between measured and predicted K_t) are normally distributed, with a 0 mean and a 0.071 standard deviation. In general, these indicators can be considered moderately good, but the graph in Figure 9 shows that the *ERDC/CHL* data lie systematically at the borders of the cloud. This is confirmed by the standard error, which for the *ERDC/CHL* data (0.091) is nearly twice that of the *QUCERL* data (0.062 for *BS-2* and 0.049 for *BS-3*).

Figure 9. Corrected Armono's model vs. the entire data base.

This would suggest that Armono's approach somehow fails in capturing the mean features of the interaction between waves and modules. For this reason, the 2 data sets respond to the predictive variables in different ways. A supplementary application of the *AVP*, not shown here for the sake of

Journal of Waterway, Port, Coastal, and Ocean Engineering. Submitted April 22, 2013; accepted September 13, 2013;
posted ahead of print September 16, 2013. doi:10.1061/(ASCE)WW.1943-5460.0000237

brevity, revealed that neither h_s/d nor (surprisingly), h_s/B_{bR} are the main sources of the observed un-homogeneity, but rather wave steepness. The latter is a leading quantity for the *QUCERL* experiments (the value of R^2 in Figure Fig. 7c is 0.60), whereas it seems to have much less influence on the *ERDC/CHL* experiments. As wave steepness is a major variable in the dissipation processes (e.g., wave breaking), it is reasonable to conclude that *BS-1* differs from *BS-2* and *BS-3* in the mechanisms that rule the attenuation of the incoming waves. However, as for most of empirical formulae, the interpretation of the scatter in terms of physical processes is not ever simple.

The conceptual approach (CA)

After investigating the properties of Armono's equation, a supplementary method is tested, namely the *conceptual approach* (*CA*), proposed by *Buccino and Calabrese* (2007), for conventional breakwaters. An interesting peculiarity of the *CA* is that the predictive equations have been deduced theoretically, although on the basis of a very simplified calculation scheme. As a consequence, the parameters of the design curves have a clear physical meaning and this makes it easier to individuate, account for and explain the different responses of the datasets. In this respect, *CA* inherently assumes the relationship between K_t and the main predictors to vary depending on the relative submergence (wave height to crest freeboard ratio). This behavior would be the consequence of a change in the dissipation mechanism that would occur when the water depth over which waves propagate reduces. Hence, if the arguments provided at the end of the previous paragraph were correct, this feature of the model may aid to achieve more uniformly reliable predictions.

However, reducing the scatter of Figure 9 is not the only concern of the analysis presented below. The data are also used to understand whether the functional forms obtained using the simplified theory of *CA* are valid for submerged breakwaters in *RB*s. The data can also be used to estimate the range of validity.

Journal of Waterway, Port, Coastal, and Ocean Engineering. Submitted April 22, 2013; accepted September 13, 2013;
posted ahead of print September 16, 2013. doi:10.1061/(ASCE)WW.1943-5460.0000237

Review of CA for underwater barriers

In the case of submerged breakwaters, the *CA* uses the energy balance equation and assumes breaking waves to be the main dissipation mode. The energy loss is macroscopically modeled using the bore-like breaker approach, originally suggested by *Le-Mehautè* (1963). After some algebra, a nonlinear differential equation is derived, which links the transmission coefficient to the main structure and wave quantities, such as the crest level R_c (difference between still water depth and structure height, taken positive), the crown width B, the incident significant wave height H_{si} and the peak period T_p. The differential equation has been found to have two asymptotic solutions. The first applies to the case of deeply submerged breakwaters, where $R_c/H_{si} >> 1$, and reads as follows:

$$K_t = \frac{1}{\left(K^s_{t0}\right)^{-1} + G_1 \frac{B}{\sqrt{H_{si} L_{0p}}} \left(\frac{H_{si}}{R_c}\right)^{1,5}} \tag{9}$$

where L_{0p} is the deepwater peak wavelength and G_1 is a dissipation factor; K^s_{t0} is the transmission coefficient for $B = 0$, i. e., for triangular barriers. The second asymptotic solution can be obtained for the opposite case, structures with the crest close to the SWL ($R_c/H_{si} << 1$). Under those conditions the solution is as follows:

$$K_t = \left(\sqrt{K^n_{t0}} - G_2 \frac{B}{\sqrt{H_{si} L_{0p}}}\right)^2 \tag{10}$$

which is totally independent of the relative submergence R_c/H_{si}. Eq. (10) represents a parabola in which the transmission coefficient, after having reached zero, increases with the crown width. Since this is an unrealistic solution, *Buccino and Calabrese* (2007) suggested to cut it horizontally at a certain large value of $\frac{B}{\sqrt{H_{si} L_{0p}}}$, B^*, beyond which K_t is reduced to few percent (e.g., less than 5%), resulting in the following:

$$K_t = \left[\sqrt{K^n{}_{t0}} - G_2 \min\left(B^*, \frac{B}{\sqrt{H_{si} L_{0p}}} \right) \right]^2 \tag{10b}$$

The basic idea of the *CA* is that Eq. (9) should hold as long as the relative submergence is larger than a certain threshold (e.g., $R_c/H_{si} \geq S_1$), whereas Eq. (10) should be valid below a second limit value ($R_c/H_{si} \leq S_2$). In between, a linear interpolation is suggested, which returns the classical form as follows:

$$K_t = a \cdot \frac{R_c}{H_{si}} + b \tag{11}$$

introduced by *van der Meer* (1990).

Altogether the model has 6 parameters to be calibrated, namely the two K_{t0}, the two G, S_1 and S_2.

For conventional rubble mound breakwaters a value of $S_1 = 0.83$ has been estimated, and S_2 is set equal to 0. For G_1 and G_2, the values of 0.33 and 0.25, respectively, have been inferred. As far as K_{t0} is concerned, a slight dependence on R_c/H_{si} has been found for deeply submerged breakwaters and $K^n{}_{t0}$ has been shown to be related to the Iribarren number. Finally, caution is suggested in using Eq. (9) for $R_c/H_{si} > 2$, because in those conditions, wave breaking is improbable.

Calibration for barriers in Reef Ball units

The *CA* model is adjusted to the case of barriers made of *Reef Balls* (the *BS* configurations). Compared to conventional structures, the calibration procedure might be, in principle, simpler because the values of K_{t0} are expected to be approximately 1; in the present situation K_{t0} corresponds to the transmission rate of a single row of *Reef Balls*, which can affect the incoming waves only slightly. This obvious reasoning was also confirmed by the observation of the *BS-1a* data for $n = 1$.

Journal of Waterway, Port, Coastal, and Ocean Engineering. Submitted April 22, 2013; accepted September 13, 2013;
posted ahead of print September 16, 2013. doi:10.1061/(ASCE)WW.1943-5460.0000237

Regarding the applicability of the model, the *CA* is expected to work more efficiently for more probable wave breaking cases. That is, for small structure submerged depths. However, for *RB* barriers the effect of macroporosity should also be considered. These effects are twofold. The large porosity tends to delay wave breaking occurrence, such that the bound $R_c/H_{si} = 2$ suggested for conventional breakwaters will be reduced. Also, the large eddies which originate at the holes of the modules produce additional energy losses, which should be accounted for. The mechanism by which wave energy is converted into turbulence is qualitatively similar to that of wave breaking, where two wide vortexes, customarily called the *plunger vortex* and the *surface roller* (*Basco, 1985*), are primarily responsible for dissipation. It is then physically plausible to include the effects of macro-porosity in the loss indexes *G* in Eqs. (9) and (10). This approach is conceptually similar to that used, among others, by *Zelt and Raichelen* (1990), who studied wave run-up at plane beaches using the Boussinesq equations and parameterized wave breaking with an artificial viscosity term in the momentum balance.

The *breaking coefficient* of the bore-like breaker approach, to which *G* is strongly related in the *CA*, is the ratio between the mean dimension of the dissipating vortex (or vortexes) and the wave height.

Furthermore, a clue that *CA* is somehow capable of capturing energy losses generated by macroroughness can be found in a recent work of *Lorenzoni et al.* (2010). The authors investigated the performances of a coastal defense structure consisting of a series of steel blades normal to the wave motion. For each cell formed by nearby blades, wave energy was drained dominantly by means of two large-scale counterrotating vortexes with horizontal axes. After comparing different transmission models (including *van der Meer ,1990*, and *van der Meer et al., 2005*), the authors verified that *CA* best fitted the experimental data, also because of a more realistic dependence on wave steepness.

Yet, the observation of those data, which were more scattered than that expected, suggest that for the dependence of K_t on the predicting variables to be properly satisfy, wave breaking should

Journal of Waterway, Port, Coastal, and Ocean Engineering. Submitted April 22, 2013; accepted September 13, 2013; posted ahead of print September 16, 2013. doi:10.1061/(ASCE)WW.1943-5460.0000237

however take place, so that its effects to those macroporosity sum. For larger submerged depths, where the importance of wave breaking is less, the data scatter is expected to increase, even if the predictions remain realistic.

Redefinition of Variables

The different characteristics of the *RBs* relative to common armor units, as well as the heterogeneity of the investigated configurations, made it necessary to redefine the main structural variables involved in the transmission process. Although this step introduces a certain degree of subjectivity, it proved very useful to develop a single prediction model, which is valid for all the layouts.

A *nominal crown width* (B_t) is defined as follows. When the modules at the top of the structure turn to an upwards convex position (normal position, layouts *BS-1* and *BS-3*), then B_t = (*n-1*) D_R. On contrary when *RBs* are placed with bacement upwards (e.g. layout *BS-2*) $B_t = n\ D_R$. The definition of B_t does not consider the gaps between the units.

The *equivalent structure height*, h_{se}, is introduced, and the corresponding *equivalent crest level, R_{ce}* as follows:

$$R_{ce} = d - h_{se} \tag{12}$$

For the layout *BS-1* (Figure 1.a), h_{se} coincides with the height of the units ($h_{se} = h_{RB}$). As far as *BS-2* is concerned (Figure 1.d), the actual structure height is given as follows:

$$h_s = \phi_p \cdot 2 \cdot h_{RB} \tag{13}$$

where φ_p is a layer thickness coefficient. However, since the modules at the top turn their empty sections to the waves, the effective crest freeboard is larger than the simple geometric submerged depth, $R_c = d - h_s$. It is expected to be halfway between R_c and R_c+h_{RB}; it is reasonably set as follows:

$$\begin{cases} R_{ce} = R_c + \dfrac{h_{RB}}{2} \\ h_{se} = h_{RB} \cdot \left(2 \cdot \varphi_p - 0.5\right) \end{cases} \tag{14}$$

Finally, because the layout *BS-3* originates from *BS-2* after adding a third level of *RBs* in the normal position, h_{se} is set as follows:

$$h_{se} = h_{RB} \cdot \left(2 \cdot \phi_p - 0.5\right) + h_{RB} = h_{RB} \cdot \left(2 \cdot \phi_p + 0.5\right) \tag{15}$$

<u>*Calibration of Eq. (10)*</u>

In a plane defined by $B_t/(H_{si}\ L_{0p})^{0.5}$ as the abscissa and $(K_t)^{0.5}$ as the ordinate, Eq. (10) represents a straight line of intercept $(K^n_{t0})^{0.5}$ and slope G_2. Thus, the validity of this asymptotic solution was preliminarily tested by plotting the data in that plane and checking the linear trend visually. Additionally, R^2 was calculated as an indicator of the goodness of fit. In general, a satisfactory agreement was found for $R_{ce}/H_{si} \leq 0.4$, but the data were scattered because of the different responses from the different layouts. This problem could be solved by assigning a dissipation index to each arrangement. In this work we have chosen the alternative (but equivalent) approach of correcting the extent of the structure B_t; because the available data are relatively few, this technique seemed to the authors to be significantly more efficient. Then an *effective crown width* is defined as follows:

$$B_t^* = \nu \cdot B_t \tag{16}$$

where the *configuration factors*, ν , vary according to Table 6. Figure 10 shows how this method results in a satisfactory grouping of the data around the line mathematically expressed as follows:

$$\sqrt{K_t} = -0.2496 \frac{B_t^*}{\sqrt{H_{si} L_{0p}}} + 0.9474 \tag{17}$$

with $R^2 = 0.90$.

Journal of Waterway, Port, Coastal, and Ocean Engineering. Submitted April 22, 2013; accepted September 13, 2013;
posted ahead of print September 16, 2013. doi:10.1061/(ASCE)WW.1943-5460.0000237

Figure 10. Experimental data vs. Eq. (17).

The dissipation coefficient, practically 0.25, is identical to that found for conventional breakwaters, while K^n_{t0} equals approximately 0.9, according to the preliminary hypotheses formulated at the beginning of this paragraph.

With respect to the values of v, Table 6 shows that, after fixing an unitary value for the case of single layer arrangement with no spacing among the modules (*BS1-e*), the coefficient reduces to 0.6 for spaced units (*BS1-a*). This is likely because of a weakening of the breaker vortexes caused by the increase of the mean depth over which waves propagate. For wide spacing in the cross-shore direction (alternate rows, *BS-1b* to *BS1-d*), v remains the same probably because of the limited structure width compared to the wavelength. However, when the units have wide gaps also in the alongshore direction (*BS-1f*), the coefficient drops to 0.25, meaning a much lower dissipation efficiency. Regarding the multilayered configurations (*BS-2* and *BS-3*), the values are larger than 1; even though this finding could be conditional on the crest freeboard re-definition, it seems to confirm that a first significant difference between the *QUCERL* and the *ERDC/CHL* data originates from the different dissipation powers of the structures. The most intuitive explanation could be the effect of the macro-roughness, because, in the multilayer structures, the number of holes capable of producing vortexes increases. The results show that v is slightly larger for *BS-2* than for *BS-3*, which seems contradictory. A possible reason might be that in the former, large vortexes take place at the bases of the upside-down modules, which dissipate a significant amount of energy because of their large diameter; when a third layer is added, these large vortexes are prevented and their effect would be only partly compensated by the additional eddies at the lateral surface of the new row. However, also the circulation which is activated among the modules and its interaction with the incoming breakers should have some effect on the global dissipation rate; though no hypotheses can be formulated at the present state of knowledge.

Journal of Waterway, Port, Coastal, and Ocean Engineering. Submitted April 22, 2013; accepted September 13, 2013;
posted ahead of print September 16, 2013. doi:10.1061/(ASCE)WW.1943-5460.0000237

Table 6. Values of the configuration factor.

The values of v in Table 6 are globally consistent with those of b_0 in Table 5; this was expected as the two parameters play the same role from the methodology point of view.

To verify the main hypotheses of Eq. (10), the data is examined to show that (a) a linear link exists between $B_t/(H_{si}\ L_{0p})^{0.5}$ and $(K_t)^{0.5}$ and (b) the role of the submerged depth, R_c, is negligible. The residuals $e = (K_{t,meas.})^{0.5} - (K_{t,calc.})^{0.5}$ were plotted versus the relative structure width (Figure 11.a) and the relative submerged depth (Figure 11.b). Since neither of the graphs exhibits a clear trend, the hypotheses cannot be rejected, although it is clear that more data are needed to better support them. This is especially true for R_{ce}/H_{si}, for which a small funnel-shaped structure (etheroschedasticity?) may be seen in the data.

However, at the present stage of the research the Eq. (17) is considered tentatively correct.

Figure 11. Residuals of Eq. (17) vs. relative structure width (a) and relative submerged depth (b).

Calibration of Eq.(9)

Eq. (9) is function of two variables, namely the relative structure width and the relative submerged depth. For conventional breakwaters, the data of the *Seabrook and Hall* (1998) experiments were used to check the dependence on each variable; in those tests both the crown extent and the crest level were systematically varied (in a wide range) under the same wave conditions.

In the present case, the data are insufficient to repeat the same procedure and consequently an alternative approach has been used. We note preliminarily that Eq. (9) can be reduced to a linear form by introducing the following variables:

Journal of Waterway, Port, Coastal, and Ocean Engineering. Submitted April 22, 2013; accepted September 13, 2013; posted ahead of print September 16, 2013. doi:10.1061/(ASCE)WW.1943-5460.0000237

$$\begin{cases} Y = \dfrac{1}{K_t} \\ \\ Z = \left(\dfrac{H_{si}}{R_{ce}}\right)^{1,5} \dfrac{B_t^*}{\sqrt{H_{si} L_{0p}}} \end{cases} \tag{18}$$

Since a single row of modules ($B_t = 0$) hardly leads to a significant reduction of the incoming wave height, we may expect the data to arrange according to the following equation:

$$Y = 1 + B \cdot Z \tag{19}$$

Thus, the experimental data have been first divided into groups, depending on the value of the *breaker index*, H_{si}/R_{ce}, (between 0.3 and 0.4, between 0.4 and 0.5, etc.). Then they have been progressively plotted on the plane (*Z, Y*) to try to understand where they might agree with Eq. (19). As shown in Figure 12a, in the interval $0.29 \leq H_{si}/R_{ce} < 0.68$ the data exhibit a certain curvature; according to the discussion provided at the beginning of the paragraph, this may be justified by the fact that the probability of wave breaking is low and then the dependence of K_t on the leading variables is not really respected. In the interval (0.68-1.1), Eq. (19) is reasonably verified (Figure 12b; $R^2 = 0.90$) and remains so up to a value of approximately 1.4 (Figure 12c; $R^2 = 0.88$).

Figure 12. Experimental data in the plane Z-Y: (a) $H_{si}/R_{ce} \leq 0.68$; (b) $0.68 \leq H_{si}/R_{ce} < 1.10$; $0.68 \leq H_{si}/R_{ce} \leq 1.40$; $0.68 \leq H_{si}/R_{ce} \leq 2.00$.

For higher values of the breaker index, the relationship between *Z* and *Y* becomes non-linear (Figure 12d).

Journal of Waterway, Port, Coastal, and Ocean Engineering. Submitted April 22, 2013; accepted September 13, 2013;
posted ahead of print September 16, 2013. doi:10.1061/(ASCE)WW.1943-5460.0000237

On the basis of the previous discussion, Eq. (9) is tentatively valid for *breaker indexes* between 0.68 and 1.4, i.e., for *relative submerged depths*, R_{ce}/H_{si}, between 0.71 and 1.47. The calibrated form is as follows:

$$K_t = \frac{1}{1 + 0.3 \cdot \left(\frac{H_{si}}{R_{ce}}\right)^{1,5} \frac{B_t^*}{\sqrt{H_{si} L_{0p}}}} \tag{20}$$

where the dissipation factor, 0.3, is similar to that found for conventional breakwaters (0.33). In Eq. (20), the variable $B^*_t/(H_{si}\ L_{0p})^{0.5}$ includes the *configuration factors*, *v*, introduced in the previous paragraph. The minimum breaker index for Eq. (20) to be strictly valid (0.68) is 36% larger than that estimated for conventional breakwaters, i.e., 0.5. As stated above, this delay in wave breaking occurrence is likely because of the larger porosity of the barriers.

To verify the correctness of the model, the data is examined to check the dependence of K_t on $(H_{si}/R_{ce})^{1.5}$ and on $B^*_t/(H_{si}\ L_{0p})^{0.5}$. Eq. (9) was first made linear as follows:

$$Y' = m + nX' + qX'' \tag{21}$$

where:

$$\begin{cases} Y' = \ln\left(\frac{1}{K_t} - 1\right) \\ X' = \ln\left(\frac{H_{si}}{R_{ce}}\right) \\ X'' = \ln\left(\frac{B_t^*}{\sqrt{H_{si} L_{0p}}}\right) \end{cases} \tag{22}$$

Journal of Waterway, Port, Coastal, and Ocean Engineering. Submitted April 22, 2013; accepted September 13, 2013; posted ahead of print September 16, 2013. doi:10.1061/(ASCE)WW.1943-5460.0000237

Then, a regression analysis was performed, at a 5% significance level. The best fit values of the parameters *n* and *q* are expected to be near 1.5 and 1, respectively. Results of the regression analysis are summarized in Table 7.

Table 7. Results of the Regression Analysis.

The p-values (column IV) are far lower than 0.05, ensuring that, unlike that found in the previous paragraph, both the relative submerged depth and the relative structure width are significant to the prediction of K_t. Moreover, columns V and VI report the 95% confidence intervals of the parameters *m, n* and *q*. The bands were calculated after checking the normality of the residuals (see next paragraph). The data show that *n* is included in the interval (1.27-2.21), whereas *q* ranges from 0.81 to 1.09; because the theoretical values (1.5-1) are internal to the bands, the hypotheses of the model cannot be rejected and Eq. (20) may be tentatively considered correct. As far as the parameter *m* is concerned, its value varies between -1.29 and -1.08, which approximately corresponds to *ln* (0.3).

<u>*The general model for the BS layouts and its properties*</u>

After the calibrations discussed above, the general predictive model for the *BS* layouts becomes the following:

$$K_t = \frac{1}{1+0.3R^{*-1,5}b^*} \qquad \text{for } 0.71 \le R^* \le 1.47 \quad (23a)$$

$$K_t = \left(-0.249 \cdot \min\left(4; b^*\right) + 0.9474\right)^2 \qquad \text{for } R^* \le 0.4 \quad (23b)$$

$$K_t = \alpha \cdot R^* + \beta \qquad \text{for } 0.4 \le R^* \le 0.71 \quad (23c)$$

where the variables:

$$\begin{cases} b^* = \dfrac{B_t^*}{\sqrt{H_{si} L_{0p}}} \\ \\ R^* = \dfrac{R_{ce}}{H_{si}} \end{cases} \tag{24}$$

must be calculated according to the definitions given in the Eqs. (12)-(15).

In Eq. (23b) an upper limit of 4 has been introduced, which corresponds to the zero of the parabola; however, more data are needed to test the validity of that formula for large values of b^* (e.g., > 2).

Predicted and measured values of the transmission coefficient are compared in Figure 13. The data show good agreement, apart from the two outliers in *BS-2*, circled in red. These data exhibit a high K_t in spite of the relatively low submerged depth ($R^* = 0.5$) and large value of b^* (between 2 and 3). However, an overall R^2 of 0.90 is calculated, which indicates a good prediction and is 10 percentage points larger than that found for the corrected Armono's equation (Fig.9).

Figure 13. Comparison between calculated and measured transmission coefficients. Dotted lines correspond to 90% confidence intervals.

The residuals are Gaussian (Figure 14), with a mean of zero and a standard deviation equal to 0.054. This value is nearly 32% smaller than that of Eqs. (7) – (8), but is slightly larger than that found for conventional breakwaters (0.047). Yet, after removing the two outliers, a value of 0.049 is obtained, which is in satisfactory agreement with previous findings.

Figure 14. Normal plot of standardized residuals.

Journal of Waterway, Port, Coastal, and Ocean Engineering. Submitted April 22, 2013; accepted September 13, 2013;
posted ahead of print September 16, 2013. doi:10.1061/(ASCE)WW.1943-5460.0000237

The *standard error* is similar for the three layouts, being i.e., 0.0520 for *BS-3*, 0.0598 for *BS-2* (including the outliers, 0.0455 without) and 0.0502 for *BS-1*. The values relative to the *QUCERL* data-sets are only slightly larger than those of the "original" Armono's formula (Eq. (1)), which gives 0.044 for BS-3 and 0.048 for BS-2. With respect to this, it is useful to remark that from the normality of residuals follows that a 0.01 difference in the standard error produces a variation of 1.64% in the 90% probability confidence semi-band.

Altogether the results above seem to indicate that, the *CA* is capable of capturing the specific response of the datasets as well as the systematic differences between them. This depends not so much on the configuration factor *v*, which is included also in Armono's equation, as on a different modeling of the effects of the submerged depth. Practically speaking, the *CA* assumes that the *QUCERL* and the *ERDC/CHL* data behave differently because the former refer to structures more submerged than the latter (on average), also because of the presence of the upside-down units. Most of the data used for the calibration of Eq. (9) were from the *QUCERL* tests, whereas the opposite was true for Eq. (10). This partitioning of data is from the one side a positive feature, as it leads to explain the possible reasons of the observed discrepancies; but from the other side it represents the primary source of uncertainty of the present analysis, which must be verified through new experiments. However, as a partial support of the findings in this study, when the few *ERDC/CHL* data with $1.47 \geq R^* \geq 0.71$ are plotted on Armono's plane *X-Y* (Figure 15), they approximately follow a straight line, in agreement with Eq. (1). This would suggest that Armono's equation realistically approximates the *RBs* behavior when the submerged depth of the reef is relatively high. In this regard, the mathematical structure of Eq. (9) is similar to Eq. (1), though the variables are different.

For values of R^* larger than 1.47, which would theoretically correspond to a negligible probability of breaking, the *CA* still gives good estimates of the transmission coefficient (Figure 16). This would confirm a certain capability of the method of capturing the effects of macro-roughness, as

Journal of Waterway, Port, Coastal, and Ocean Engineering. Submitted April 22, 2013; accepted September 13, 2013; posted ahead of print September 16, 2013. doi:10.1061/(ASCE)WW.1943-5460.0000237

concluded by *Lorenzoni et al.* (2010). However, the graph shows the points to be slightly s-shaped as a consequence of the lack robustness in the dependence on the predicting variables (lack of linearity in Figure 12a). In some cases, transmission coefficients larger than 1 were observed. This may be either the effect of an incorrect measurement or the result of a strong nonlinear interaction between the waves and the reef (see e.g., *Massel, 1983*).

Figure 15. *ERDC/CHL* data for deeply submerged reefs in Armono's plane (Eqs. (1) and (2)).

Figure 16. Calculated vs. measured K_t for $R^* > 1.47$.

Reef Balls on top of a mound

Experiments with *Reef Balls* placed on the crest of a rubble mound (160 tests in all, layouts *B-P1*, *B-F1* and *B-F2*) were carried out only at the *QUCERL* lab. Similar to the *BS* geometries, some potentially influential variables were constant in the tests; among them, the crest width (B_m) and the front slope angle (α_{off}) of the berm (see Figure 1d for reference). Because of this limitation in the data, a new calibration was not performed. Accordingly, a different approach was used.

Physically, the rubble mound is expected to have almost no effect on the transmission coefficient if it is low; otherwise, as the berm height (h_m) increases, the structure response will begin to resemble that of a conventional breakwater.

The boundary between <u>low mounds</u> and <u>high mounds</u> has been empirically reached when the height of the berm approximately equals its submerged depth. More precisely, for $F/h_m \geq 0.95$ (Figure 1d), Eqs. (23) still reasonably predict K_t; this is shown in Figure 17, where the 90% confidence intervals

Journal of Waterway, Port, Coastal, and Ocean Engineering. Submitted April 22, 2013; accepted September 13, 2013; posted ahead of print September 16, 2013. doi:10.1061/(ASCE)WW.1943-5460.0000237

(±0.088) are also shown for comparison. Nearly 12% of the 105 data points plotted in the graph exceeds the bands; this would be in line with that found for the *BS* layouts.

Figure 17. Eqs. (23) vs. bermed layouts with low mound.

Yet, most of the data is below the lower bound, indicating a slight overprediction. This is likely the effect of the berm, which reduces the permeability of the whole structure (berm + *RB*s), thus increasing both reflection and dissipation.

Figure 18. (a) Eqs. (23) vs. bermed layouts with high mound;

(b) the same data vs. Eqs. (24) and (25).

For $F/h_m < 0.95$, the prediction method for *BS* layouts is no longer valid (Figure 18a). As stated before, in this case, the response should not be much different than that of a conventional breakwater. Consistently, the system *rubble mound + Reef Balls* is modeled as a well submerged conventional breakwater with submerged depth F and crown width B_m. The *RB*s are supposed to be an *added resistance*, which increases the rate of wave energy dissipation (from both wave breaking and macroroughness). Thus, the following predictive equation is derived:

$$K_t = \frac{1}{1.18 \cdot \left(\frac{H_{si}}{F}\right)^{0,12} + G_R \cdot \left(\frac{H_{si}}{F}\right)^{1,5} \frac{B_m}{\sqrt{H_{si} L_{p0}}}} \tag{25}$$

which is the same as for conventional breakwaters, except for the dissipation factor, G_R, which accounts for the role of the *RB* units. Based on the analysis of the *B-P1* and *B-F*1 layouts (55 data points), the following expression was found:

Journal of Waterway, Port, Coastal, and Ocean Engineering. Submitted April 22, 2013; accepted September 13, 2013;
posted ahead of print September 16, 2013. doi:10.1061/(ASCE)WW.1943-5460.0000237

$$G_R = 0.33 \cdot \exp\left(\frac{n \cdot D_R}{B_m}\right) \tag{26}$$

where the exponential term represents the percentage of the berm crown occupied by the *RB*s. The comparison with the data is shown in Figure 18b. Eqs. (25) and (26) are assumed to be valid in the range $0.6 \leq F/H_{si} \leq 3.5$,which is broader than that for conventional breakwaters.

Altogether, the proposed procedure for layouts of type *B* has proven as reliable as the original Armono's equation; it gives a $R^2 = 0.90$ vs. the value of 0.92 for Eqs. (1)-(2).

Only for the layouts *B-F1* and *B-P1*, *Armono and Hall* (2003) proposed a different model as follows:

$$K_t = 1.616 - 31.322 \cdot \left(\frac{H_{si}}{gT_p^{\ 2}}\right) - 1.099 \cdot \left(\frac{h_s}{d}\right) + 0.265 \cdot \left(\frac{h_s}{B_{bR}}\right) \tag{27}$$

Eq. (27) did not perform as well as the proposed procedure based on the *CA*, having an R^2 equal to 0.85 vs. 0.90 for the proposed approach (calculated only on *B-F1* and *B-P1*).

Conclusions

This study analyzed more than 300 experimental data points of wave transmission for submerged breakwaters using *Reef Balls*^{TM}, to develop reliable design tools for the prediction of the transmission coefficient, K_t, which is the ratio between the wave height directly behind the barrier and that directly in front of it.

Although wave attenuation is only one of the phenomena that a structural solution provides to defend a shore (there is also wave induced circulation, wave diffraction, sand trapping and many others), K_t represents a leading indicator of the capability of the structure to dissipate the incoming wave energy. Therefore, it is significant from an engineering point of view.

Journal of Waterway, Port, Coastal, and Ocean Engineering. Submitted April 22, 2013; accepted September 13, 2013; posted ahead of print September 16, 2013. doi:10.1061/(ASCE)WW.1943-5460.0000237

The data base used in this study is comprised of two series of physical model tests conducted at the *Queen's University Coastal Engineering Research Laboratory* (*QUCERL*, Canada) and at the USACE *Engineering Research and Development Center Coastal and Hydraulics Laboratory* (*ERDC/CHL*, USA). To the authors knowledge, those experiments represent, to date, the only systematic investigations performed on the topic.

The *QUCERL* data have been previously analyzed by *Armono* (2002) and *Armono and Hall* (2003), who proposed. The sole design equations available till now (Eqs. (1) and (27)). The *ERDC/CHL* experiments are practically discussed in this paper for the first time, even though the tests were completed in the early 2000s.

Different arrangements of the modules have been examined ; some of them are of an immediate practical interest (one-layer bottom-seated and bermed arrangements, *BS-1*, *B-F1* and *B-P1*), whereas some others (multilayered configurations, *BS-2*, *BS*-3 and *B-F2*) may represent stimulating solutions for future research and development.

A detailed review of Armono's equation was provided. Even after eliminating the features of the formula from which a lack of fit might originate and re-adjusting the model to the entire data base, the *ERDC/CHL* data showed scatter around the prediction line more than the *QUCERL* data (Figure 9). This would indicate that the predicting variables selected by Armono, along with the functional relationship which links them, do not explain enough about the physics that govern the wave transmission process.

To address this problem, the *conceptual approach* (*CA*), suggested by *Buccino and Calabrese* (2007), was selected as an alternative model. The following three reasons led to this choice:

a) The equations of the *CA* were deduced theoretically and the parameters of the predictive curves have a physical meaning that can aid the interpretation of results;

Journal of Waterway, Port, Coastal, and Ocean Engineering. Submitted April 22, 2013; accepted September 13, 2013;
posted ahead of print September 16, 2013. doi:10.1061/(ASCE)WW.1943-5460.0000237

b) The relationship between K_t and the main variables changes depending on the degree of submergence. The functional form is then not unique, which may explain the discrepancies between the *QUCERL* data and the *ERDC/CHL* data; and

c) Although derived for conventional rubble mound breakwaters, the model provided realistic predictions of K_t, even for structures dissipating wave energy by macroroughness (*Lorenzoni et al., 2010*). The latter represents an important result in understanding *RB* functioning.

The calibration of the *CA* for bottom-seated layouts (*BS-1, BS-2* and *BS-3*) led to Eqs. (23a)-(23c). An ad hoc residuals diagnostic carried out on the asymptotic solutions (Eqs. (9) and (10)) showed that the model appropriately fit the data (Figure 11 and Table 7) . A value of the R^2 statistic equal to 0.90 was found and the residual scatter was approximately the same for all the arrangements (the overall standard error equals 0.054, see Figure 13). This is one of the strong points of the *CA* and is primarily an effect of point b) of the list above. The *QUCERL* data behaved differently from the *ERDC/CHL* data because the structures are on average more submerged. This is caused by the use of the upside-down units.

Another very important parameter of the model is the *configuration factor, v* (Eq. 16). With its introduction, the dissipation indexes G_1 and G_2 of Eqs. (9) and (10) are split into the product of two terms; one is a coefficient identical to that used for conventional breakwaters and the other (v) accounts for the specific dissipative properties of a given *RB* arrangement, including the effects of macroporosity .

For <u>*single layer layouts,*</u> v was set equal to 1 in the case of no spacing among the modules; then it was found to reduce up to 0.25 for broadly spaced units (Table 6). As far as the <u>*multilayer configurations*</u> are concerned, indexes larger than 1 have been estimated; this result may be explained of course by a larger dissipation from macro-roughness, but it also partially depends on the crest level redefinition associated with the presence of the upside-down modules (Eqs. (14)-

Journal of Waterway, Port, Coastal, and Ocean Engineering. Submitted April 22, 2013; accepted September 13, 2013;
posted ahead of print September 16, 2013. doi:10.1061/(ASCE)WW.1943-5460.0000237

(15)). Given the non-linear nature of the relationship between K_t and b^* (Eqs. (23)), the introduction of gaps among the units, or a change to multilayer arrangements, does not result in an uniform variation of the structure performance. The effects would be more significant for wide barriers (b^* approximately 2-3) with the crest close to the mean water level, whereas the impact on short and/or well-submerged structures would be more limited. Since the data representing large breakwaters with a small submerged depth were few, this issue must be investigated through new experiments.

Some support for these results findings can be inferred because Eqs. (23) hold also for *bermed configurations* with low mounds ($F/h_m \geq 0.95$, Figure 1d). This achievement (Figure 17) is physically consistent and indicates that the predictive equations are robust. The approach used for high mounds, where *RBs* are included as an adjunctive resistance at the top of the barrier, is useful (Figure 18), but needs to be extended also to situations where $F < 0.6$. To this scope additional tests are needed

In Figure 19, the performance of a conventional breakwater (panel a) are compared to those of a barrier of *RBs* placed on a low berm (panel b). The mean water depth is assumed to be 3 m and the submerged depth is fixed at 0.5 m; the slopes of the mound are both 1:2. The significant wave height is assumed to be 1.8 m (incipient breaking condition), with a peak period of 7 s. In panel c, the transmission coefficient is plotted vs. the structure width. The results show that using *RBs*, less energy is dissipated because of the larger porosity and of the absence of acute slopes that would enhance wave breaking. But with 7 rows, the incoming wave height is reduced by 50%, which may be appropriate for many situations of practical interest. With a conventional breakwater, the same target could be reached with a crown width of 5 m, but the amount of rock to quarry would be significantly larger; under the ideal situation depicted in the graph (homogeneous mounds with 0.4 porosity) *RBs* would save nearly 611 cubic meters of rock per 100 m of barrier length, i.e., 40% of the material employed for the conventional structure.

Figure 19. Conventional breakwater vs. a composite *RB* barrier. The values of K_t for the conventional breakwater have been estimated by *Buccino and Calabrese* (2007).

This represents a good environmental advantage, which would add to the naturalistic and aesthetic advantages. In addition, the large permeability of the *RBs* might also reduce the intensity of the alongshore current associated with the pumping of water mass over the barrier, as described in many recent papers (e.g. *Lamberti et al., 2007, Vicinanza et al., 2009 and Calabrese et al., 2011*).

Previous reasoning, although necessarily rough, serves to support the idea that *RBs* may represent an effective option for shore erosion control. This is even more true considering the fact that the cost of modules (currently of the order of 1,000 Euros each in Europe) could significantly lower due to the larger number of units employed compared to pure environmental enhancement projects. However many aspects of both the functional and the structural response of *Reef Balls* are still to be investigated.

Acknowledgments

The authors wish to gratefully acknowledge Dr. H.D. Armono and Dr. Donald L. Ward for providing the experimental data analyzed in this work.

References

Armono, H.D., 2002. Hemispherical Shaped Artificial Reefs. Dissertation. Queen’s University, Kingston, Ontario, Canada, 2003.

Journal of Waterway, Port, Coastal, and Ocean Engineering. Submitted April 22, 2013; accepted September 13, 2013; posted ahead of print September 16, 2013. doi:10.1061/(ASCE)WW.1943-5460.0000237

Armono, H.D., Hall, K.R., 2003. Wave transmission on submerged breakwaters made of hallow hemispherical shape artificial reefs. Proceedings of 31st annual conference of the Canadian Society for Civil Engineering.

Basco, D., 1985. Qualitative description of wave breaking (motion patterns).Journal of Waterway, Port, Coastal and Ocean Engineering 111 (2),171e188 (ASCE).

Barber, R.T., 2001. Reef Balls™: An Anvanced Technique to Mimic Natural Reef System using Designed Artificial Reefs. www.artificialreefs.org/scientificreports/ReffBallProjectPlanning.htm.

Briganti, R., van der Meer, J.W., Buccino, M., Calabrese, M., 2004. Wave transmission behind low-crested structures. Proceeding of Coastal Structures 2003, 580-592.

Buccino, M., Calabrese, M., 2007. Conceptual Approach for Prediction of Wave Transmission at Low-Crested Breakwaters. Journal of Waterways, Port, Coastal and Ocean Engineering, 133 (3), 213-224.

Burcharth H.F., Hawkins T., Zanuttigh B., Lamberti A., 2007. Environmental Design Guidelines for Low Crested Coastal Structures.

Calabrese, M., Di Pace, M., Buccino, M., Tomasicchio, G.R., Ciralli, E. 2011. Nearshore circulation at a coastal defence system in Sicily. Physical and numerical experiments. Journal of Coastal Research ISSUE 64: 474-478.

d´Angremond, K., van der Meer, J.W. e De Jong, R..J., 1996. Wave transmission at low-crested structures. Proceedings of International Conference of Coastal Engineering, 3305-3318.

Draper, N.H., Smith, H., 1981. Applied Regression Analysis. John Wiley and sons.

Goda, Y., Ahrens, J.P., 2008. New Formulation on Wave Transmission Over and Through Low-Crested Structures. Proc of 31st International Conference on Coastal Engineering, 3530-3541.

Journal of Waterway, Port, Coastal, and Ocean Engineering. Submitted April 22, 2013; accepted September 13, 2013; posted ahead of print September 16, 2013. doi:10.1061/(ASCE)WW.1943-5460.0000237

Harris, L.E., 2007. Designed Reefs Coastal Stabilization and Reef Restoration. www.artificialreefs.org.

Lamberti A., 2005. Editorial Paper on *DELOS* project. Coastal Engineering 52, 815-818.

Lamberti, A., Martinelli, L., Zanuttigh, B., 2007. Prediction of wave induced water flow over and through the structure, of set-up and rip-currents. In: Environmental Design Guidelines for Low Crested Coastal Structures, Section 13.5. Elsevier, Amsterdam.

Le Mehautè, B. 1963. On non-saturated breakers and wave run-up. Proc. 8th Conf. on Coastal Engineering, 77–92.

Lorenzoni, C., Soldini, L., Brocchini, M. Mancinelli., Postacchini, M., Seta, E., Corvaro, S., 2010. Working of Defense Coastal Structures Dissipating by Macroroughness. Journal of Waterways, Port, Coastal and Ocean Engineering. 136, 77-90.

Massel, S.R., 1983. Harmonic generation by waves propagating over a submerged step. Coastal Engineering, 7, 357-380.

Seabrook, S. R., e Hall, K. R., 1998. Wave transmission at submerged rubble mound breakwaters. Proceedings International Conference on Coastal engineering, 2000–2013.

Tanaka, N. 1976. Effects of submerged rubble-mound breakwater on wave attenuation and shoreline stabilization. Proc. Japanese Coastal Engineering Conf. JSCE, Tokyo, 152–157 (in Japanese).

Tomasicchio, G.R., D'Alessandro, F., 2013. Wave energy transmission through and over low-crested breakwaters. Journal of Coastal Research, SI 65: 398-403.

van der Meer, J.W., 1990. Low crested and reef breakwaters. Technical report n.H986II, Delft Hydraulics.

van der Meer, J.W., Briganti, R., Zanuttigh, B., Wang, B., 2005. Wave transmission and reflection at low-crested structures: design formulae, oblique wave attack and spectral change. Coastal Engineering 52 (10–11), 915–929.

Vicinanza, D.,Caceres, I., Buccino, M., Gironella, X., Calabrese, M., 2009. Wave disturbance behind low crested structures: diffraction and overtopping effects. Coastal Engineering, 56, 1173-1185.

Ward, D.L., 2012. Physical Model Study of an Experimental Reef Ball™ Breakwater for Miami Beach, Florida. Contract Report submitted to U.S. Army Engineer Research and Development Center, Coastal and Hydraulics Laboratory, Vicksburg, MS.

Zelt, J.A. and Raichlen, F., 1990. A lagrangian model for water induced harbour oscillation. Journal of Fluid Mechanics, 213, 203-225.

Figure1

Journal of Waterway, Port, Coastal, and Ocean Engineering. Submitted April 22, 2013; accepted September 13, 2013; posted ahead of print September 16, 2013. doi:10.1061/(ASCE)WW.1943-5460.0000237

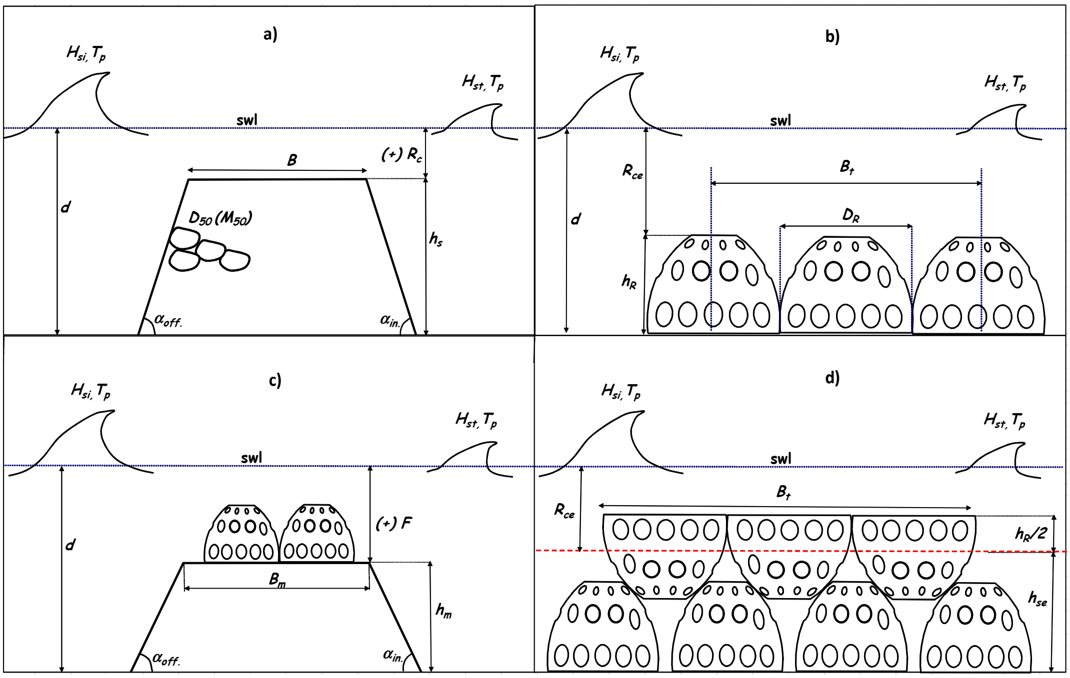

Figure2

Journal of Waterway, Port, Coastal, and Ocean Engineering. Submitted April 22, 2013; accepted September 13, 2013; posted ahead of print September 16, 2013. doi:10.1061/(ASCE)WW.1943-5460.0000237

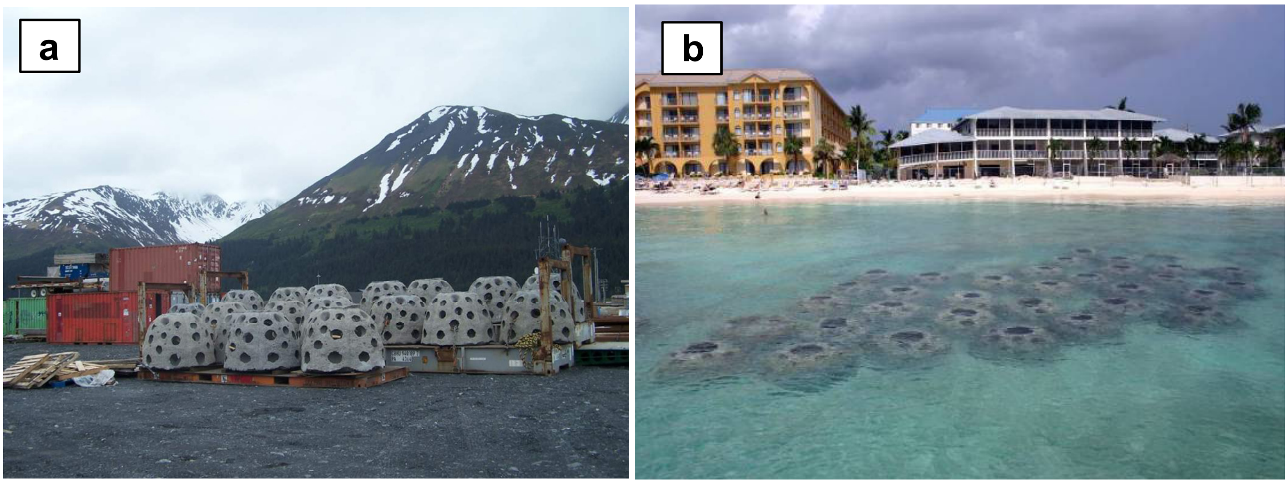

Figure3

Journal of Waterway, Port, Coastal, and Ocean Engineering. Submitted April 22, 2013; accepted September 13, 2013; posted ahead of print September 16, 2013. doi:10.1061/(ASCE)WW.1943-5460.0000237

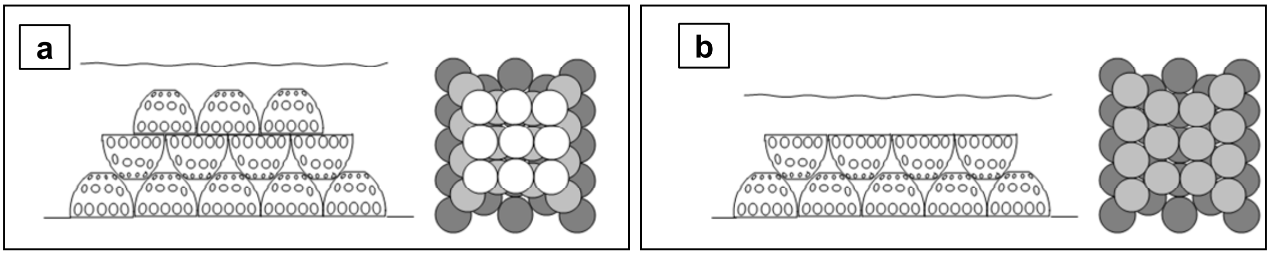

Figure4

Journal of Waterway, Port, Coastal, and Ocean Engineering. Submitted April 22, 2013; accepted September 13, 2013; posted ahead of print September 16, 2013. doi:10.1061/(ASCE)WW.1943-5460.0000237

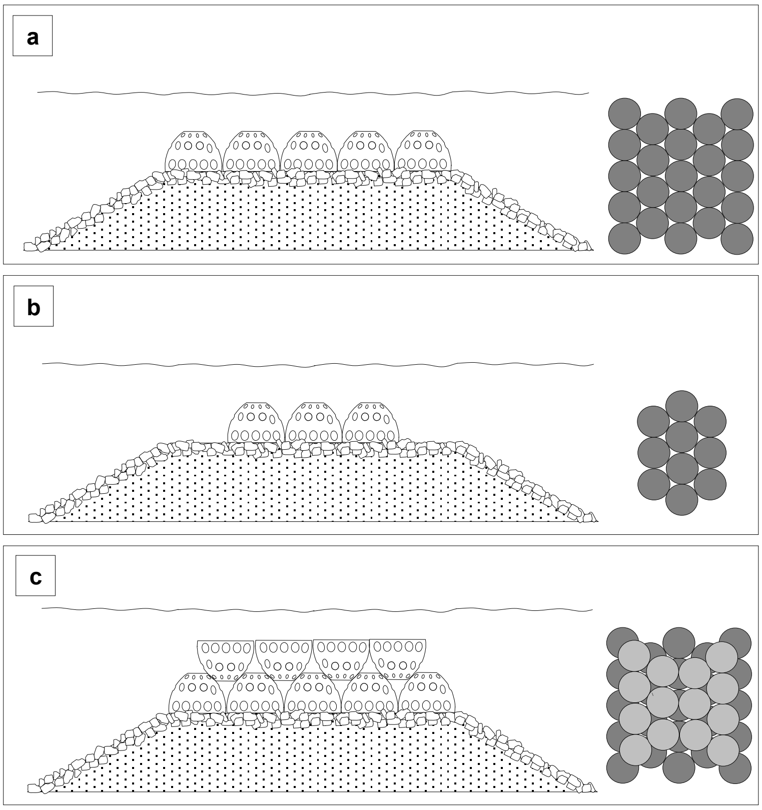

Figure5

Journal of Waterway, Port, Coastal, and Ocean Engineering. Submitted April 22, 2013; accepted September 13, 2013; posted ahead of print September 16, 2013. doi:10.1061/(ASCE)WW.1943-5460.0000237

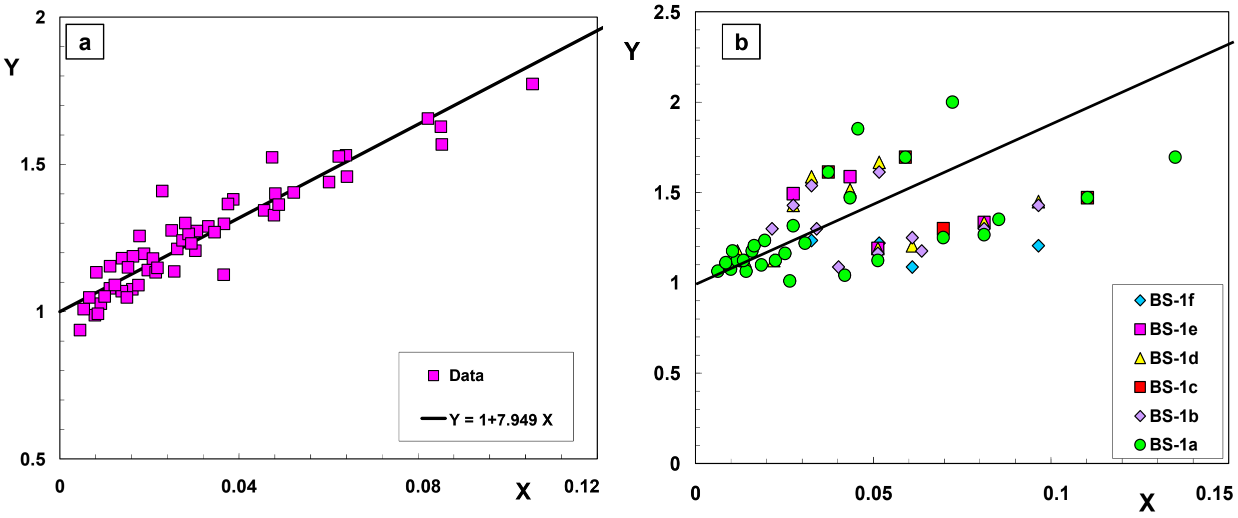

Figure6

Journal of Waterway, Port, Coastal, and Ocean Engineering. Submitted April 22, 2013; accepted September 13, 2013; posted ahead of print September 16, 2013. doi:10.1061/(ASCE)WW.1943-5460.0000237

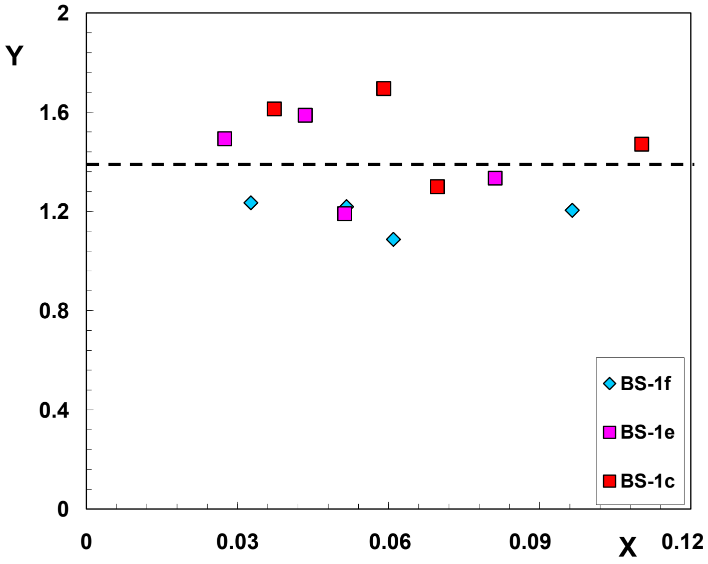

Figure7

Journal of Waterway, Port, Coastal, and Ocean Engineering. Submitted April 22, 2013; accepted September 13, 2013; posted ahead of print September 16, 2013. doi:10.1061/(ASCE)WW.1943-5460.0000237

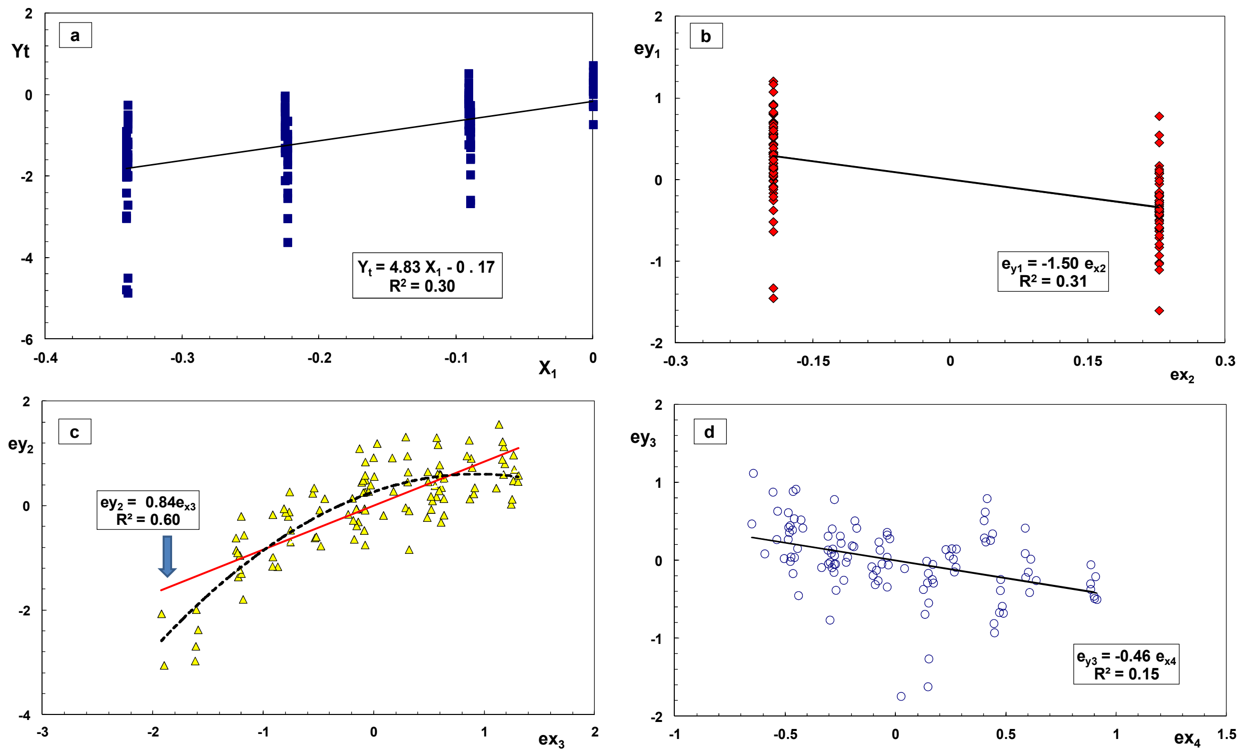

Figure8

Journal of Waterway, Port, Coastal, and Ocean Engineering. Submitted April 22, 2013; accepted September 13, 2013; posted ahead of print September 16, 2013. doi:10.1061/(ASCE)WW.1943-5460.0000237

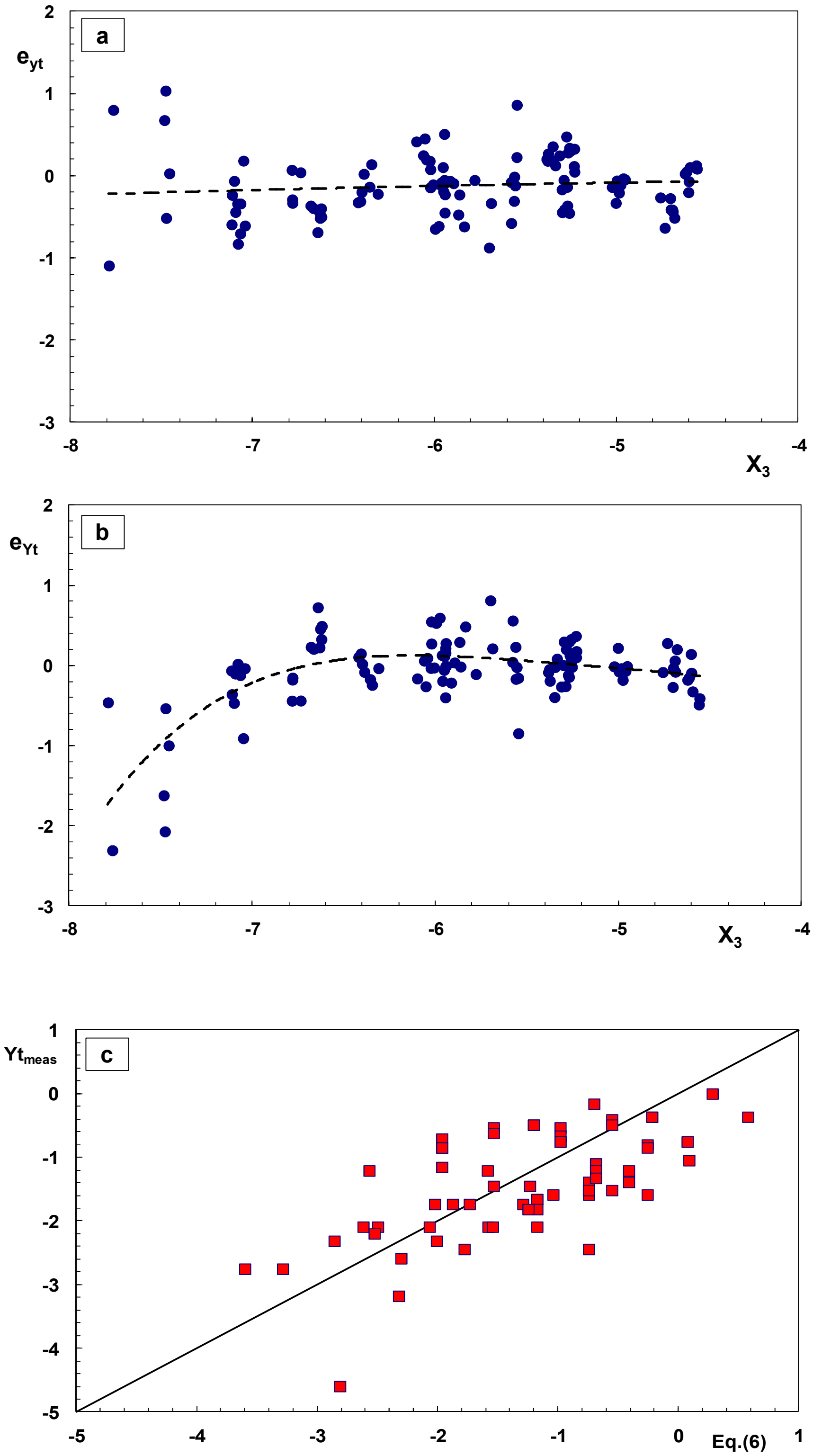

Figure9

Journal of Waterway, Port, Coastal, and Ocean Engineering. Submitted April 22, 2013; accepted September 13, 2013; posted ahead of print September 16, 2013. doi:10.1061/(ASCE)WW.1943-5460.0000237

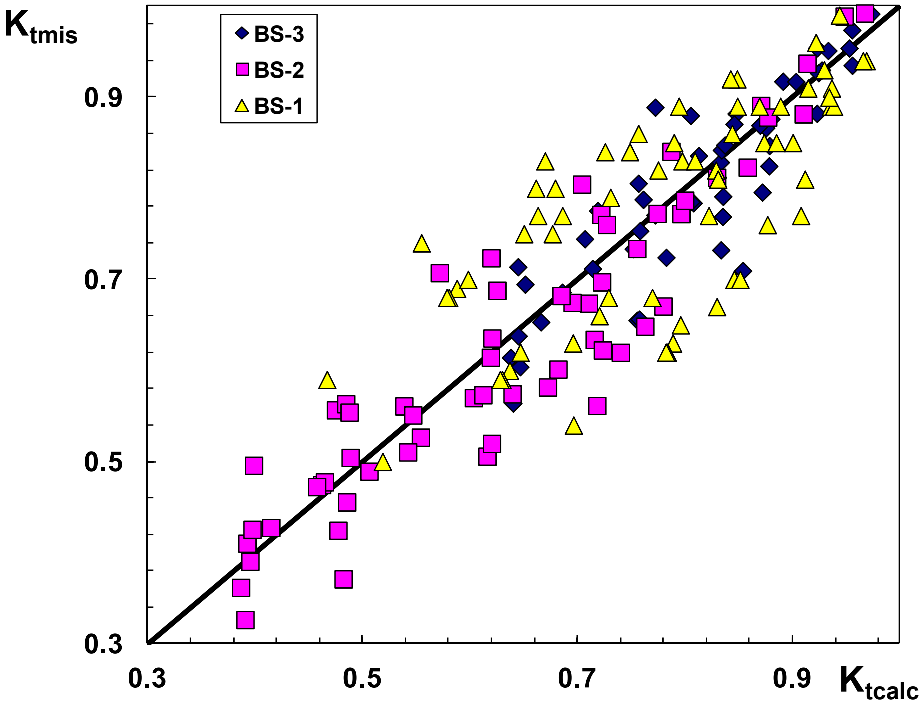

Figure10

Journal of Waterway, Port, Coastal, and Ocean Engineering. Submitted April 22, 2013; accepted September 13, 2013;
posted ahead of print September 16, 2013. doi:10.1061/(ASCE)WW.1943-5460.0000237

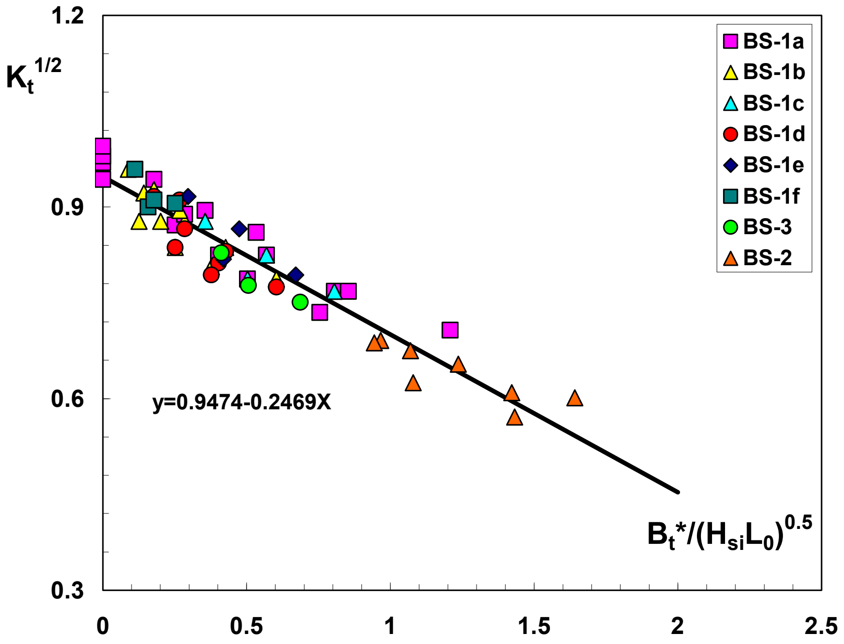

Figure11

Journal of Waterway, Port, Coastal, and Ocean Engineering. Submitted April 22, 2013; accepted September 13, 2013; posted ahead of print September 16, 2013. doi:10.1061/(ASCE)WW.1943-5460.0000237

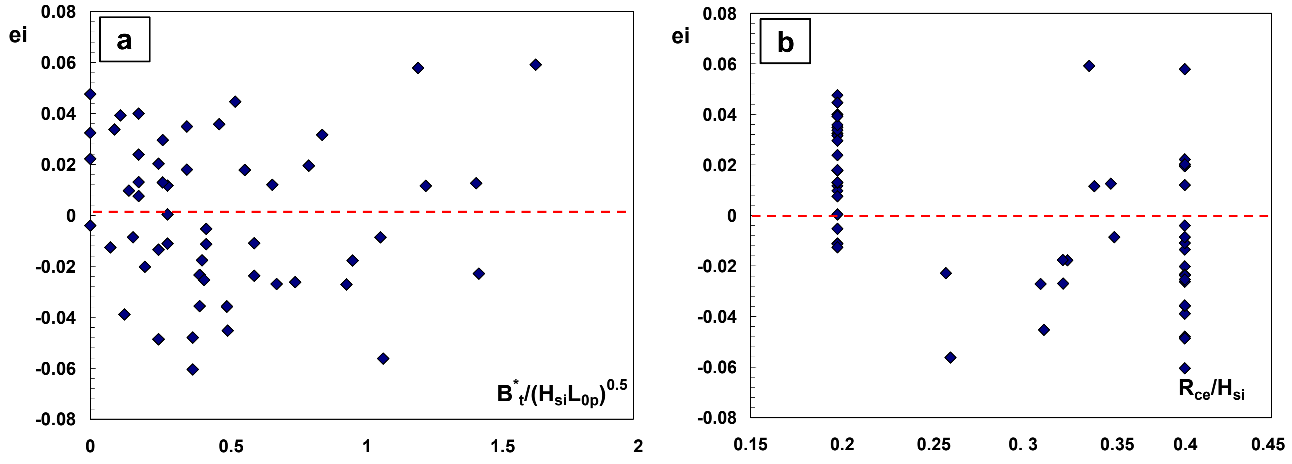

Figure12

Journal of Waterway, Port, Coastal, and Ocean Engineering. Submitted April 22, 2013; accepted September 13, 2013; posted ahead of print September 16, 2013. doi:10.1061/(ASCE)WW.1943-5460.0000237

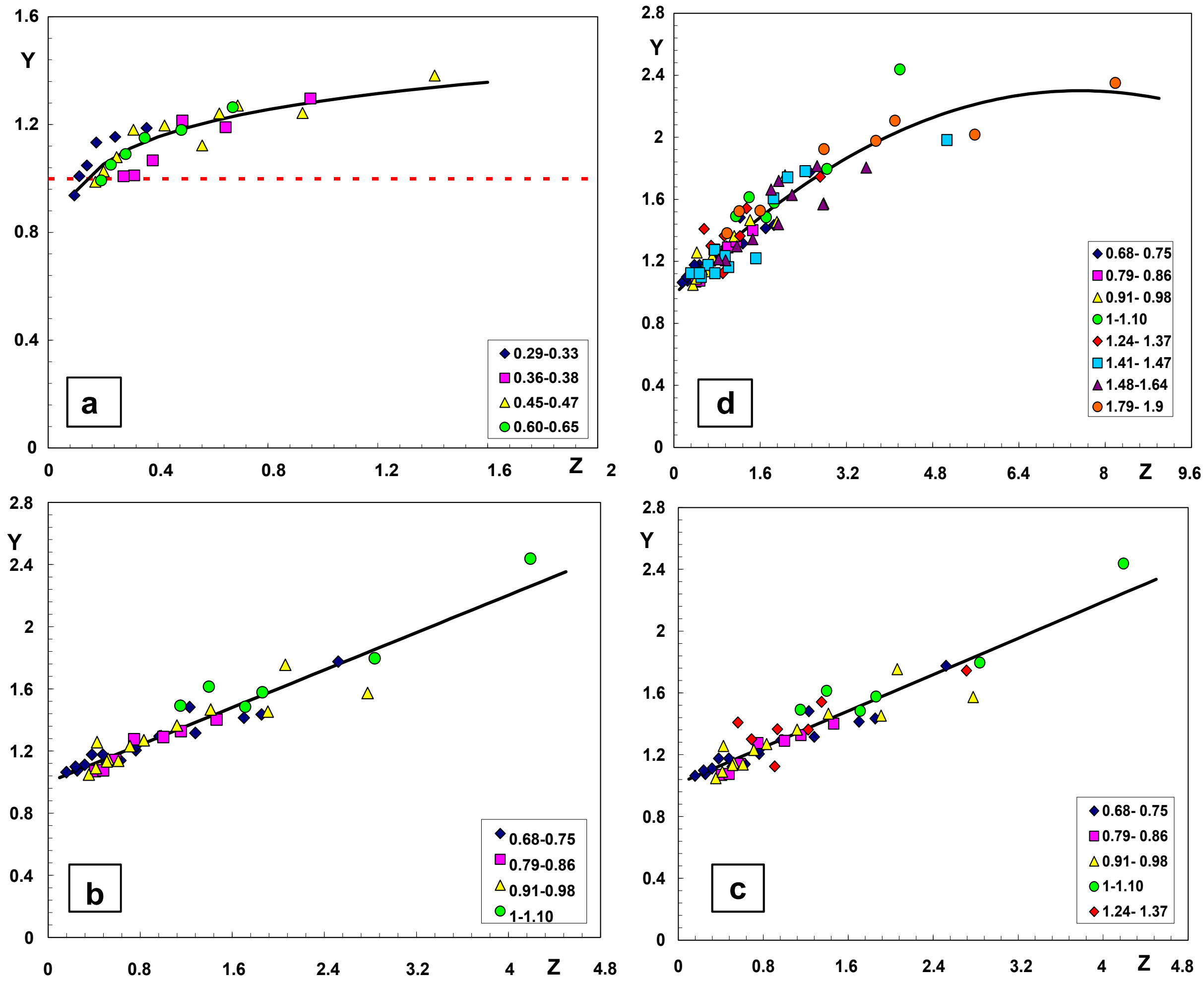

Figure13

Journal of Waterway, Port, Coastal, and Ocean Engineering. Submitted April 22, 2013; accepted September 13, 2013; posted ahead of print September 16, 2013. doi:10.1061/(ASCE)WW.1943-5460.0000237

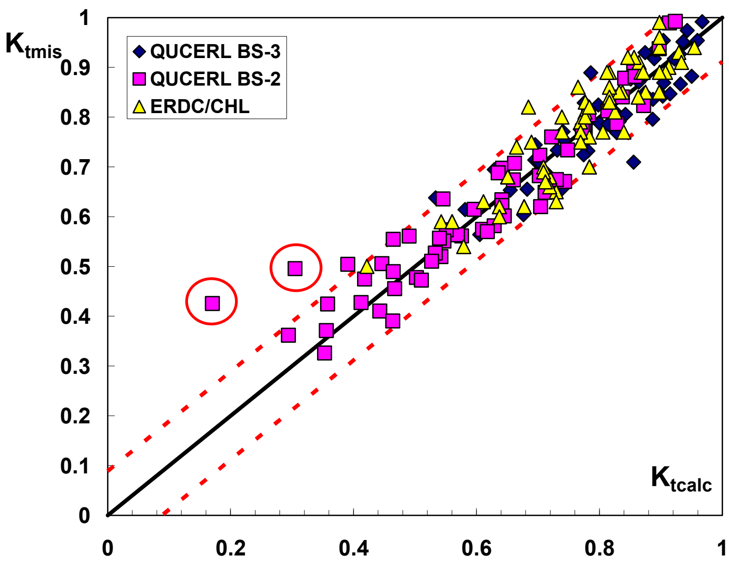

Figure14

Journal of Waterway, Port, Coastal, and Ocean Engineering. Submitted April 22, 2013; accepted September 13, 2013; posted ahead of print September 16, 2013. doi:10.1061/(ASCE)WW.1943-5460.0000237

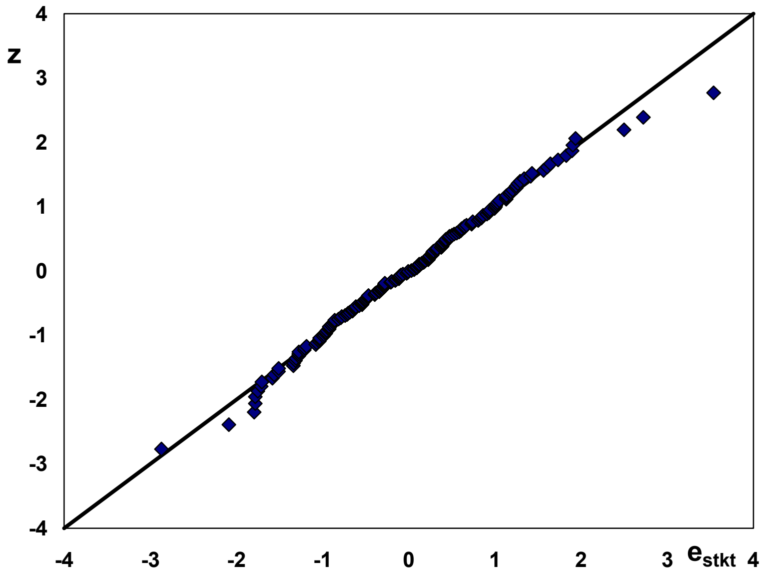

Figure15

Journal of Waterway, Port, Coastal, and Ocean Engineering. Submitted April 22, 2013; accepted September 13, 2013;
posted ahead of print September 16, 2013. doi:10.1061/(ASCE)WW.1943-5460.0000237

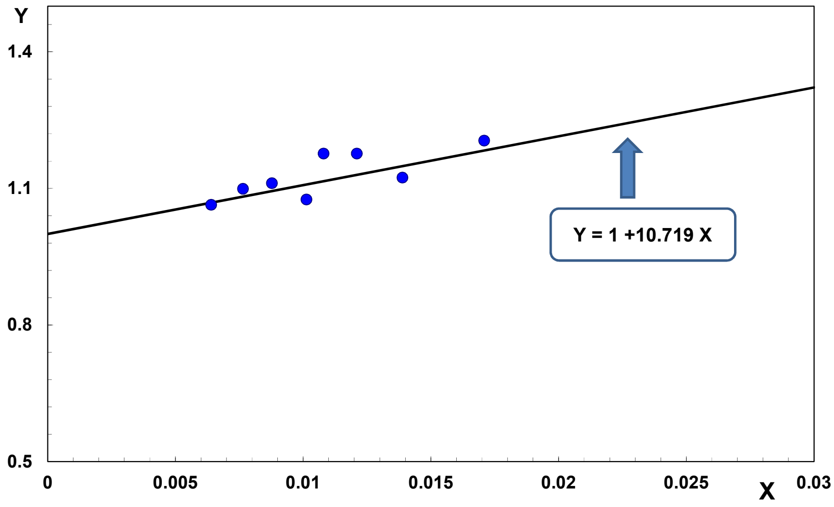

Figure16

Journal of Waterway, Port, Coastal, and Ocean Engineering. Submitted April 22, 2013; accepted September 13, 2013;
posted ahead of print September 16, 2013. doi:10.1061/(ASCE)WW.1943-5460.0000237

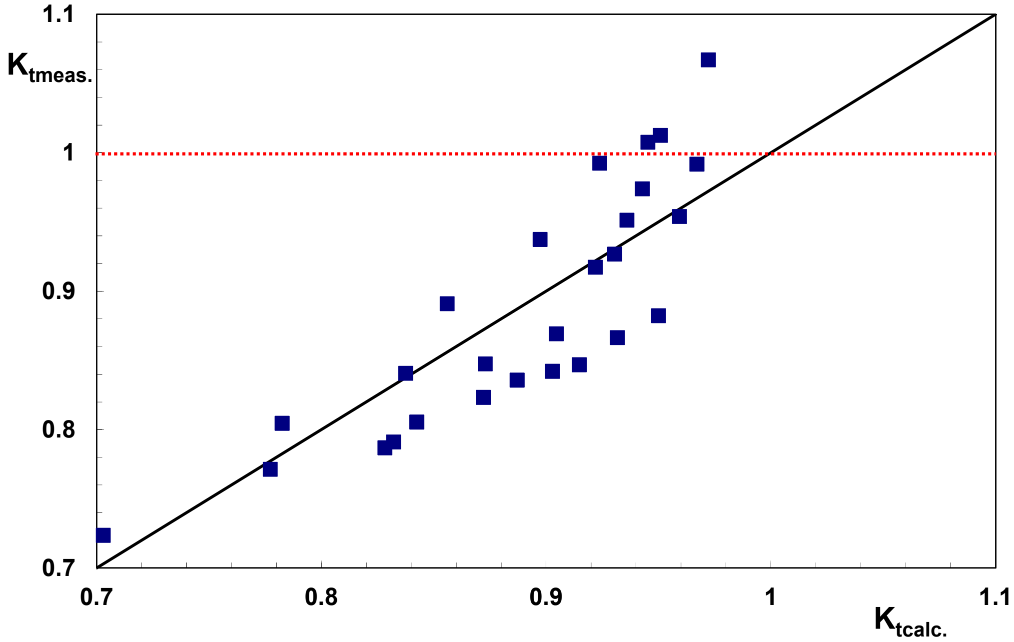

Figure17

Journal of Waterway, Port, Coastal, and Ocean Engineering. Submitted April 22, 2013; accepted September 13, 2013; posted ahead of print September 16, 2013. doi:10.1061/(ASCE)WW.1943-5460.0000237

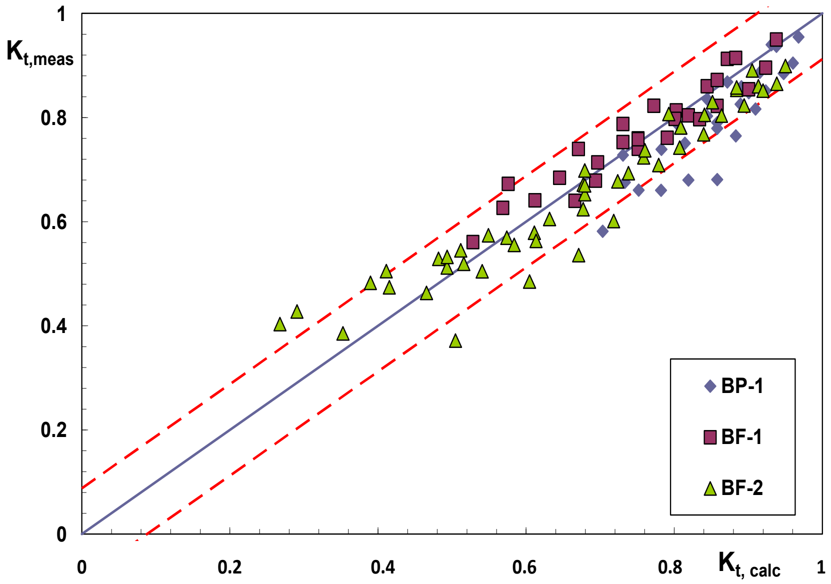

Figure18

Journal of Waterway, Port, Coastal, and Ocean Engineering. Submitted April 22, 2013; accepted September 13, 2013; posted ahead of print September 16, 2013. doi:10.1061/(ASCE)WW.1943-5460.0000237

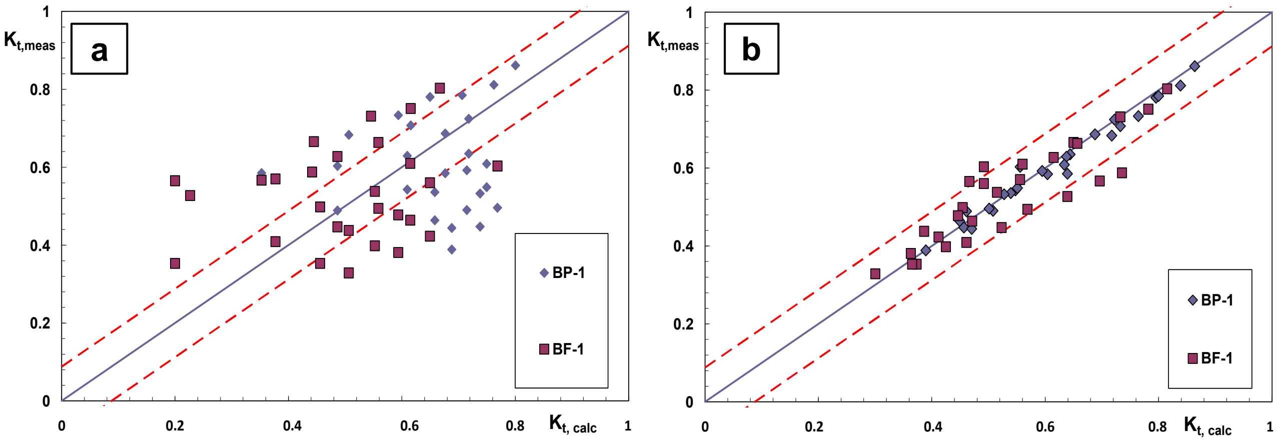

Figure19

Journal of Waterway, Port, Coastal, and Ocean Engineering. Submitted April 22, 2013; accepted September 13, 2013; posted ahead of print September 16, 2013. doi:10.1061/(ASCE)WW.1943-5460.0000237

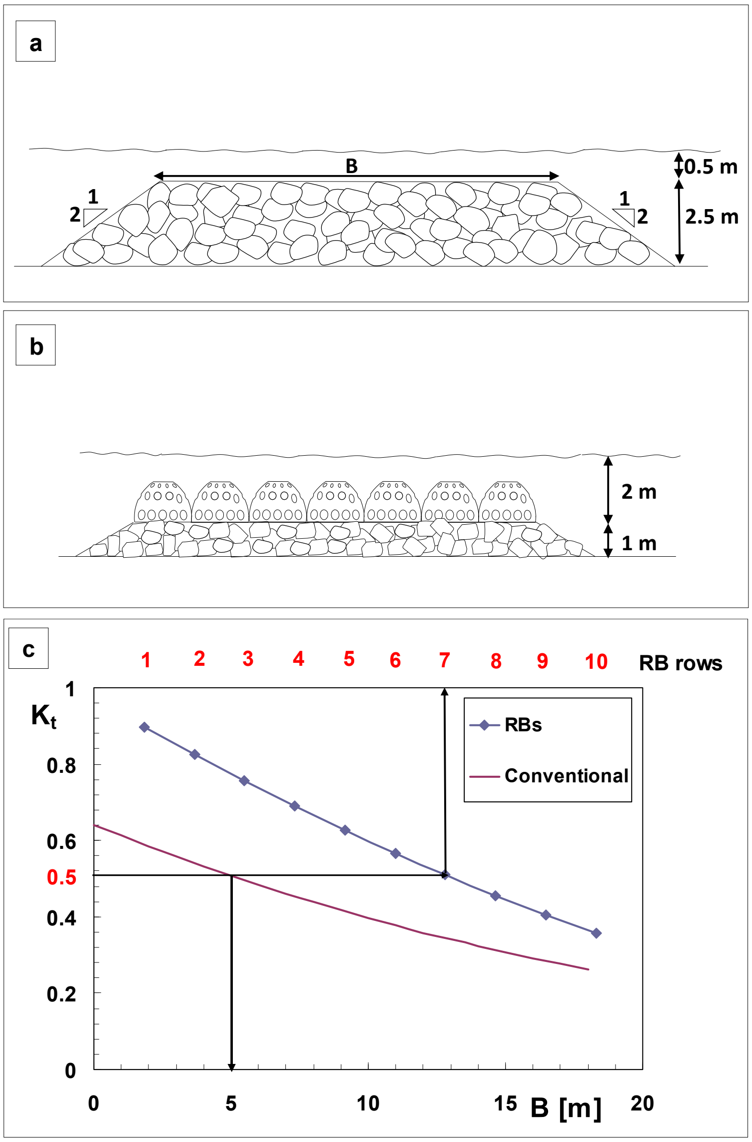

Journal of Waterway, Port, Coastal, and Ocean Engineering. Submitted April 22, 2013; accepted September 13, 2013; posted ahead of print September 16, 2013. doi:10.1061/(ASCE)WW.1943-5460.0000237

Unit Type	Base Diam. (D_R in m.)	height (h_R in m)	weight (in kg)	concrete vol. (in m^3)	# of holes
Goliath Ball	*1.83*	*1.52*	*1800-2700*	*1.0*	*25-40*
Super Ball	*1.83*	*1.37*	*1800-2700*	*1.0*	*22-34*
Ultra Ball	*1.83*	*1.31*	*1600-2000*	*0.7*	*22-34*
Reef Ball	*1.83*	*1.22*	*1350-1900*	*0.6*	*22-34*
Pallet Ball	*1.22*	*0.90*	*700-1000*	*0.25*	*17-24*
Bay Ball	*0.90*	*0.61*	*170-340*	*0.08*	*11-16*
Mini Bay Ball	*0.76*	*0.53*	*70-90*	*less than four 50 lb bags*	*8-12*
Lo Pro Ball	*0.61*	*0.46*	*35-60*	*less than two 50 lb bags*	*6-10*
Oyster Ball	*0.46*	*0.30*	*15-20*	*less than one 50 lb bags*	*6-8*

Table 1. *Reef Ball* characteristics. Source: www. Reefball.org.

Layout	# data	n	d [m]	H_{si} [m]	T_p [s]	$K_{t,meas}$
BS-3	*54*	*3*	*0.35-0.45*	*0.05-0.20*	*1.0-3.5*	*0.56-1.06*
BS-2	*60*	*4*	*0.21-0.30*	*0.05-0.20*	*1.0-3.5*	*0.33-0.99*
BF-2	*49*	*4*	*0.43-0.60*	*0.05-0.20*	*1.0-2.5*	*0.37-0.89*
BF-1	*56*	*5*	*0.35-0.50*	*0.05-0.20*	*1.0-2.5*	*0.33-0.95*
BP-1	*56*	*3*	*0.35-0.50*	*0.05-0.20*	*1.0-2.5*	*0.39-0.95*

Table 2. Synthesis of the *QUCERL* tests.

Journal of Waterway, Port, Coastal, and Ocean Engineering. Submitted April 22, 2013; accepted September 13, 2013; posted ahead of print September 16, 2013. doi:10.1061/(ASCE)WW.1943-5460.0000237

Layout name	Arrangement	# data	n	d [m]	H_{si} [m]	T_p [s]	K_{tmeas}
BS-1a	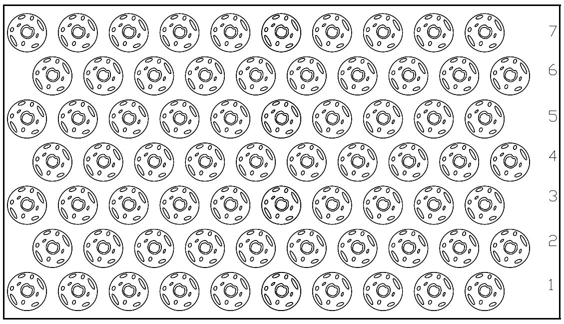	28	1 - 7	0.183 0.256	0.076 0.152	1.58 2.53	0.50 0.99
BS-1b	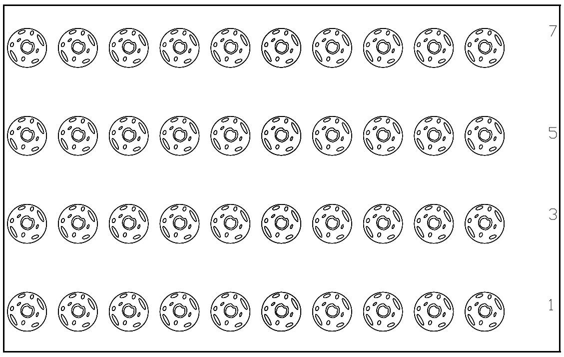	12	2 - 4	0.183	0.076 0.152	1.58 2.53	0.62 0.92
BS-1c	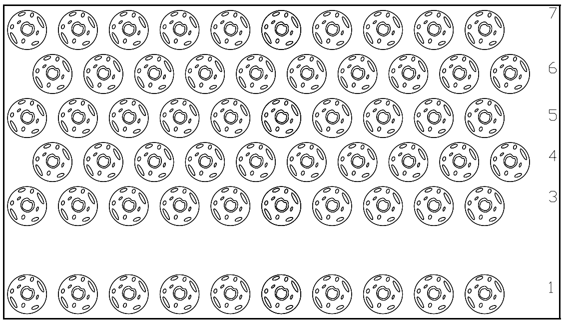	4	5	0.183	0.076 0.152	1.58 2.53	0.59 0.77
BS-1d	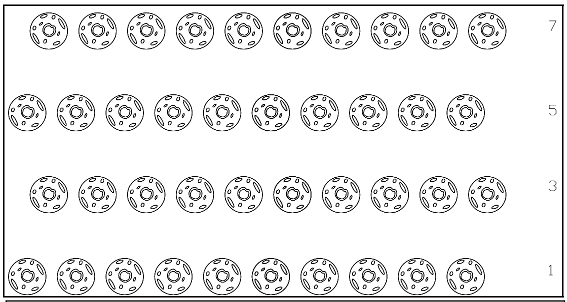	12	3 - 4	0.183 0.256	0.076 0.152	1.58 2.53	0.60 0.91
BS-1e	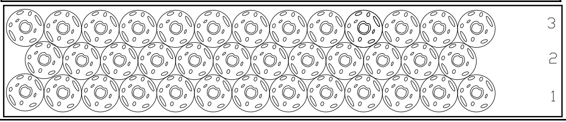	4	3	0.183	0.076 0.152	1.58 2.53	0.63 0.84

Journal of Waterway, Port, Coastal, and Ocean Engineering. Submitted April 22, 2013; accepted September 13, 2013;
posted ahead of print September 16, 2013. doi:10.1061/(ASCE)WW.1943-5460.0000237

BS-1f	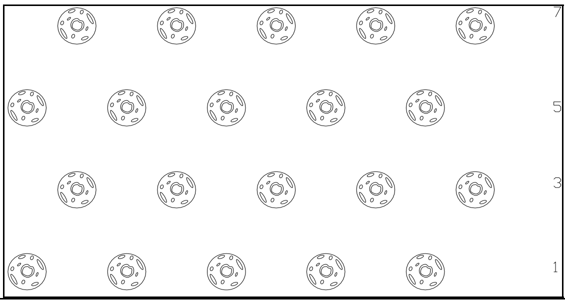	*4*	*3*	*0.183*	*0.076* *0.152*	*1.58* *2.53*	*0.81* *0.92*

Table 3. Summary of *ERDC/CHL* tests.

Layout	A_0
BS-3	*10.719*
BS-2	*7.949*
B-F2	*14.527*
B-F1	*14.527*
B-P1	*14.527*

Table 4. Values of Armono's scale factor

Layout	b_0	**Average**
BS-1a	*-9.5*	
BS-1b	*-9.29*	
BS-1c	*-9.51*	
BS-1d	*-9.24*	***-9.44***
BS-1e	*-9.13*	
BS-1f	*-10.26*	

BS-2	*-9.16*	***-9.16***
BS-3	*-9.26*	***-9.26***

Table 5. Values of the parameter a_0.

Layout	***v***
BS-1a	*0.6*
BS-1b	*0.6*
BS-1c	*0.6*
BS-1d	*0.6*
BS-1e	*1*
BS-1f	*0.25*
BS-3	*1.4*
BS-2	*1.5*

Table 6. Values of the configuration factor

	I	**II**	**III**	**IV**	**V**	**VI**
	Coefficients	*Standard Error*	*Stat t*	*p-value*	*95% Confidence bands*	
m	*-1,187*	*0,0526*	*-22,587*	*7,01x10^{-27}*	*-1,293*	*-1,081*
n	*1,736*	*0,234*	*7,4316*	*1,82x10^{-09}*	*1,266*	*2,206*
q	*0,950*	*0,069*	*13,7054*	*4,91x10^{-18}*	*0,811*	*1,090*

Table 7. Results of the Regression Analysis.